U–Pb geochronology of the Sondalo gabbroic complex (Central Alps) and its position within the Permian post-Variscan extension

B. Petri, G. Mohn, E. Skrzypek, T. Mateeva, F. Galster, G. Manatschal

▶ **To cite this version:**

B. Petri, G. Mohn, E. Skrzypek, T. Mateeva, F. Galster, et al.. U–Pb geochronology of the Sondalo gabbroic complex (Central Alps) and its position within the Permian post-Variscan extension. International Journal of Earth Sciences, 2017, 106 (8), pp.2873 - 2893. 10.1007/s00531-017-1465-x . hal-01670449

HAL Id: hal-01670449
https://hal.science/hal-01670449

Submitted on 12 Apr 2021

HAL is a multi-disciplinary open access archive for the deposit and dissemination of scientific research documents, whether they are published or not. The documents may come from teaching and research institutions in France or abroad, or from public or private research centers.

L'archive ouverte pluridisciplinaire **HAL**, est destinée au dépôt et à la diffusion de documents scientifiques de niveau recherche, publiés ou non, émanant des établissements d'enseignement et de recherche français ou étrangers, des laboratoires publics ou privés.

U–Pb geochronology of the Sondalo gabbroic complex (Central Alps) and its position within the Permian post-Variscan extension

B. PETRI[1*], G. MOHN[2], E. SKRZYPEK[3], T. MATEEVA[4], F. GALSTER[5,6], G. MANATSCHAL[1]

[1]Ecole et Observatoire des Sciences de la Terre, Institut de Physique du Globe de Strasbourg – CNRS UMR7516, Université de Strasbourg, 1 rue Blessig, F−67084, Strasbourg Cedex, France

[2]Département Géosciences et Environnement, Université de Cergy-Pontoise, 5, mail Gay Lussac, Neuville-sur-Oise, 95031 Cergy-Pontoise Cedex, France

[3]Department of Geology and Mineralogy, Graduate School of Science, Kyoto University, Kitashirakawa Oiwake−cho, Sakyo−ku, 606−8502 Kyoto, Japan

[4]Department of Earth and Ocean Sciences, University of Liverpool, Liverpool L69 3BX, United Kingdom

[5]Institute of Earth Sciences, University of Lausanne, Géopolis, CH-1015 Lausanne, Switzerland

[6]Department of Geological Sciences, University of Texas at Austin, Austin, TX-78712, USA

** Now at Institute of Earth Sciences, University of Lausanne, Géopolis, CH-1015 Lausanne, Switzerland*

Author contact: bpetri@unistra.fr

ORCID: 0000-0001-7142-0406

Short title: Austroalpine Permian evolution

REFERENCE

Petri B., Mohn G., Skrzypek E., Mateeva Ts., Galster F., Manatschal G., 2017. U–Pb geochronology of the Sondalo gabbroic complex (Central Alps) and its position within the Permian post-Variscan extension. International Journal of Earth Sciences, 106(8), 2873-2893. DOI:10.1007/s00531-017-1465-x

ABSTRACT

The end of an orogenic cycle is commonly associated with a general extensional regime, widespread magmatism and complex metamorphic overprints. The Austroalpine domain in SE Switzerland and N Italy preserves a polyphase tectonic history spanning the Carboniferous Variscan orogeny, the Late Carboniferous – Early Permian post-Variscan extension and the Jurassic rifting. In this study, the late- and post-Variscan evolution of the Austroalpine domain is explored by constraining the timing of intrusion of the Sondalo gabbroic complex in the Campo unit. U–Pb zircon dating on magmatic and metamorphic rocks and trace element geochemistry in zircon are performed using laser ablation coupled with mass spectrometry. The ages of both magmatic and metamorphic rocks range between 289 ± 4 and 285 ± 6 Ma. Trace elements in zircon from magmatic rocks indicate that zircon grew in two different chemical systems: an initial one devoid of garnet and with already crystallized plagioclase, and a second one with an increasing modal amount of garnet and lacking (initial) plagioclase. The second system probably reflects mixing of the initial magma

with melt derived from the surrounding partially molten metapelites. New results, existing age data and *P–T* estimates allow to describe the late- to post-Variscan evolution of the Austroalpine domain. These data are compared and integrated in the framework of the Permian geodynamic setting in Western Europe. We present new arguments to consider the "Permian event" in Europe as a process which was temporally distinct from the collapse of the Variscan orogen. Late-Variscan re-equilibration of the crustal thickness occurred between 310 and 290 Ma (i.e. during the collapse phase). Permian mafic magmas emplaced from 290 to 270 Ma formed either during or even after the latest stages of the Variscan collapse.

Keywords: U–Pb dating; Alps; Austroalpine nappes; Gabbro; Permian.

INTRODUCTION

The end of an orogenic cycle is generally associated with the thinning and extension of a previously thickened continental crust, which is classically referred to as orogenic collapse due to gravitational re-equilibration (e.g. Rey et al. 2001). This extension (wide rift mode; Royden and Keen 1980; Buck 1991) is commonly associated with the formation of extensional detachment faults and core complexes (Vanderhaeghe and Teyssier 2001; Whitney et al. 2012) exposing in some places partially molten continental crust. Lithospheric thinning associated with an increase of the geothermal gradient causes partial melting of the rising asthenospheric mantle and leads to the production of calc-alkaline to tholeiitic magmas (Bonin et al. 1998). Such mafic magmas will likely be pounding at the Moho, forming underplated mafic bodies (Fountain and Salisbury 1981; Fountain 1989; Rudnick and Fountain 1995) which may, in turn, cause the formation of high-temperature (HT) metamorphic rocks (Harley 1989). All these processes can interact and overlap in time and space, leading to complex overprinting relationships that characterize the post-orogenic tectono-metamorphic evolution (Whitney et al. 2012).

In Western Europe, the late- to post-orogenic extension of the Variscan orogen started in the Late Carboniferous (Burg et al. 1994) and continued during the Early Permian (e.g. Lorenz and Nicholls 1984). During the Early and Middle Permian (290–260 Ma), important lithospheric extension was associated with transtensional tectonics (Arthaud and Matte 1977), formation of sedimentary basins (Cassinis et al. 1995) controlled locally by extensional detachment faults (Froitzheim et al. 2008) as well as intense mafic and felsic magmatic activity (see e.g. Timmerman 2004; Schaltegger and Brack 2007). This magmatic activity potentially explains the rejuvenation of the lower crust (Bois et al. 1989; Costa and Rey 1995). Heat advected by mantle-derived mafic melts combined with lithospheric extension was responsible for widespread HT-metamorphism, as recorded in several parts of the Alps (Schuster and Stüwe 2008) and in Corsica (Caby and Jacob 2000). This event (Schuster et al. 2001; Schuster and Stüwe 2008) which occurred between the end of Variscan orogeny and the onset of Mesozoic rifting that ultimately led to the opening of several oceanic domains (e.g. Meliata-Vardar, Alpine Tethys and Southern North Atlantic), remains enigmatic. It is characterized by the complex interaction between extensional tectonics and magmatic and metamorphic processes that significantly modified the continental lithosphere. In particular, two issues remain debated: (1) the spatial and temporal relationship between tectonics, magmatism and metamorphism, and (2) the processes related to extension and the general geodynamic context (Lorenz and Nicholls 1984; Stampfli 1996; Henk 1999; Schuster et al. 2001; Wilson et al. 2004; Frizon de Lamotte et al. 2015).

The Alpine belt and more particularly the Austroalpine domain in SE Switzerland and N Italy represent an important natural laboratory to investigate part of this “Permian event”. Indeed the Austroalpine domain allows a direct access to distinct portions of the Permian lithosphere exhumed at or close to the surface during Jurassic rifting and subsequently involved in the Alpine orogeny (Mohn et al. 2011; 2012). The Austroalpine domain is composed of a pre-Mesozoic metamorphic basement recording a complex pre- syn- and post-Variscan tectono-metamorphic history (e.g. Maggetti and Flisch 1993; Spillmann and Büchi 1993). Late Carboniferous to Early Permian plutons emplaced in all crustal levels (Spillmann and Büchi 1993; Müntener et al. 2000; Braga et al. 2001) are associated with the deposition of

superficial volcano-sedimentary series (Von Quadt et al. 1994). In particular, the evolution and timing of magmas emplaced at mid-crustal levels during late- to post-Variscan times remain poorly constrained. Therefore, this study focuses on the Austroalpine Campo unit because (1) it escaped significant Jurassic rift-related and later Alpine deformation, and (2) it hosts the Sondalo gabbroic complex, emplaced at mid-crustal levels during the Permian (Tribuzio et al. 1999; Braga et al. 2001; Petri et al. 2016). This study brings new constraints on the emplacement age of the Sondalo gabbroic complex based on U–Pb zircon dating associated with trace-element geochemistry in zircon. Using data from the literature, these results are integrated in the late- to post-Variscan evolution of the Austroalpine and the overall Western European domain. The ultimate aim of the study is to discuss the implications of this "Permian event" for the geodynamic evolution of Western Europe during Permian time.

VARISCAN AND POST-VARISCAN EVOLUTION OF THE AUSTROALPINE DOMAIN

The Austroalpine domain in SE Switzerland and adjacent N Italy (Fig. 1) consists of Late Cretaceous top to the West nappe stack subsequently reactivated during Tertiary N-S compression (Froitzheim et al., 1994; Handy 1996). Due to the effects of minor to moderate Alpine overprint as well as Jurassic rifting (Froitzheim et al. 1994; Viola et al. 2003; Mohn et al. 2011), this domain preserves and document a polyphase pre-Mesozoic tectonic history spanning the Late Carboniferous – Early Permian post-Variscan extension and the Carboniferous Variscan orogeny. Notably, the domain provides access to distinct levels of the Permian lithosphere from the sub-continental mantle to the upper continental crust (e.g. Mohn et al. 2010). The post-Variscan evolution is characterized by widespread alkaline and tholeiitic magmatism at different crustal levels and high-grade contact to regional metamorphism locally reaching granulite facies. In contrast, the Variscan evolution of the area is characterized by calc-alkaline magmatism and high-grade metamorphism up to upper amphibolite facies conditions in some metasediments.

Variscan evolution

Variscan metamorphism is reflected by the presence, in the Ulten zone (Upper Tonale unit), of Grt–Ky migmatites recording a pressure peak of 11 kbar attained at 750 °C and 351–343 Ma, followed by a temperature peak of 750–800 °C attained at 8.5–12.5 kbar and 330–326 Ma (U–Pb on monazite; Braga et al. 2007; Braga and Massonne 2008; Langone et al. 2011). Pre-Namurian (Serpukhovian) amphibolite facies metamorphism is documented in the Err and Bernina units (Halmes 1991; Spillmann and Büchi 1993). Grt–St mica schist of the Campo unit records undated amphibolite-facies metamorphic conditions of 5–9 kbar and 550–600 °C (Braga et al. 2001; Petri et al. 2016). Calc-alkaline diorites and granodiorites were emplaced in the Bernina unit at 338–324 Ma (U–Pb on zircon multi-grain dissolution; Rageth 1984; Spillmann and Büchi 1993; Von Quadt et al. 1994) but do not show evidence for subsequent Variscan deformation (Spillmann and Büchi 1993).

Post-Variscan Permian evolution

The Permian lower crust was intruded between 281 ± 19 and 278 ± 3 Ma by mafic magmas of tholeiitic affinity. Examples are the Fedoz and the Braccia gabbros in the Margna-

Malenco units (Figs 1b and 2; U–Pb on zircon; Spillmann and Büchi 1993; Hansmann et al. 2001). They were emplaced at the crust-mantle transition zone at around 10 kbar (Hermann et al. 1997; Hermann et al. 2001). The Braccia gabbro is surrounded by HT-MP felsic granulite that consists of Grt–Ky bearing residual rocks equilibrated at 10 kbar and 800−850 °C (Hermann et al. 1997; Müntener et al. 2000). Monazite dating shows that HT conditions lasted *ca.* 20 Ma between 280 and 257 Ma (Hermann and Rubatto 2003). Crystallization of hydrous phases at around 9 kbar and 600 °C (Müntener et al. 2000), dated as Late Triassic to Early Jurassic (Villa et al. 2000), was related to the onset of rifting and subsequent exhumation of these rocks (Müntener and Hermann 2001; Trommsdorff et al. 2005).

The Permian middle crust, represented by the Campo unit, was sporadically intruded by Permian granitoids (Fig. 1b; e.g. Gazzola et al. 2000) at *ca.* 285-259 Ma as indicated by Rb–Sr ages on whole rock and mineral separates (Del Moro et al. 1981; Boriani et al. 1982; Del Moro and Notarpietro 1987). Their emplacement at $P < 4.5$ kbar is inferred from the presence of andalusite and sillimanite in their contact aureoles (e.g. Del Moro and Notarpietro 1987). Tourmaline-bearing pegmatites within the Campo basement yield Sm–Nd garnet–K-feldspar isochron ages of 255–250 Ma, Rb–Sr muscovite ages of 257−251 Ma and K–Ar muscovite ages of 217–187 Ma (Hanson et al. 1966; Thöni 1981; Sölva et al. 2003).

The Permian upper crust documents the emplacement of felsic magmatic rocks during the Early Permian. In the Bernina unit, the Carboniferous calc-alkaline suite was intruded by a 295–292 Ma alkaline syenite-granite emplaced at $P < 3$ kbar, (Figs 1b and 2; Büchi 1987; Spillmann and Büchi 1993; Von Quadt et al. 1994). Both Carboniferous calc-alkaline and Lower Permian alkaline intrusives and their host rocks are unconformably overlain by younger, 288 ± 7 Ma alkaline rhyolite (Staub 1946; Rageth 1984; Von Quadt et al. 1994).

THE SONDALO GABBROIC COMPLEX AND ITS HOST ROCK

The Sondalo gabbroic complex emplaced in the Campo unit which is delimited to the S by the Insubric line and to the NE and W by Late Cretaceous thrust faults. The Campo unit is separated from the overlying Grosina unit by the Eita shear zone (Meier 2003). This shear zone is polyphase; it was active during Jurassic rifting, was weakly reactivated during the Alpine orogeny (Fig. 3; Meier 2003; Mohn et al. 2012) and likely preserves a pre-Jurassic history (Petri 2014). The Campo unit consists of amphibolite-facies mica schist, paragneiss and minor amphibolite and calc-silicate of Ordovician protolith age (U–Pb ages on detrital zircons; Bergomi and Boriani 2012). Alpine overprints remain weak in the Campo unit, being limited to its borders (Schmid and Haas 1989; Gazzola et al. 2000).

Among the numerous Permian intrusives in the Campo unit, the Sondalo gabbroic complex is exposed over 40 km² in the N−S oriented Adda Valley (Fig. 3). The pluton is concentrically zoned; it is composed of Ol–gabbro and troctolite surrounded by gabbro and norite in the Central Zone (CZ; Fig. 4ab), and diorite to granodiorite in a Border Zone (BZ) of variable thickness (Fig. 4cde; Koenig 1964). The zone boundaries are rarely exposed. All different facies are thought to be derived from a basaltic parental liquid of tholeiitic affinity, differentiated through fractional crystallization and affected by crustal assimilation (Tribuzio et al. 1999). Sm–Nd mineral-isochrons on troctolite and norite samples gave ages of 300 ± 12 and 280 ± 10 Ma, respectively. Rb–Sr isochron ages for the same samples are respectively 266 ± 10 and 269 ± 16 Ma (Tribuzio et al. 1999). Zircon grains from a diorite sample

collected in the BZ yielded a 270 Ma upper intercept age by U−Pb multigrain dissolution dating (Bachmann and Grauert 1981).

Petrography of host metasediments

Metasedimentary rocks of the Campo unit essentially consist of Grt–St and Ms–Bt–Sil mica schist and paragneiss. They record a succession of three structures: a relictual NE–SW striking and steeply dipping foliation (S1), a main NW−SE striking and steeply dipping foliation (S2), and a foliation parallel to the pluton margins and dipping moderately away from the pluton center (S3; Fig. 3). Due to a first pre-Permian regional metamorphic event, metasedimentary host rocks reached amphibolite-facies conditions of 6 kbar/650 °C contemporaneously to the development of S1 and S2 (Petri et al. 2016). Subsequently, the Permian intrusion of the Sondalo complex variably affected the metasedimentary unit: far from the intrusion (*ca.* 10 km), heat advected by the magma caused static growth of cordierite and andalusite, attesting of heating at 3–4 kbar (sample BPA 099-12a from Petri et al. 2016). Conversely, elongated host rock xenoliths (septa) up to 300 m in thickness and 1 km in length were incorporated within the complex, while migmatization parallel to the S3 fabric occurred in the contact aureole (Fig. 3). From the host rocks to the core of the intrusion, increasing metamorphism led to the transformation of Grt–St–Ms–Bt mica schist into Grt–Sil–Bt paragneiss and Grt–Sil–Crd–Spl granulitic paragneiss which equilibrated at 5.5 kbar/930 °C. In the contact aureole, S2 was transposed into S3 at supra-solidus conditions (Figs 3 and 4f) while Grt–Sil–Bt melanosomes in the migmatitic metasediments (Fig. 4f) document similar *P–T* conditions than granulitic paragneiss between 5.2–6 kbar/500–800 °C, with a last equilibration at $P < 4.5$ kbar (Braga et al. 2001; Braga et al. 2003; Petri et al. 2016).

Petrography of the Sondalo gabbroic complex

Ol–gabbro, troctolite gabbro and norite in the CZ of the complex (Fig. 4ab) are mainly composed of euhedral to subhedral plagioclase, olivine, orthopyroxene and clinopyroxene. Plagioclase is labradoritic and often presents a more calcic core. Olivine is often replaced by talc and magnetite. Clinopyroxene is poikilitic, sometimes rimmed by red-brown Ti–pargasite that may also be poikilitic. Both pyroxene and pargasite are sometimes transformed into brown-green hornblende. Interstitial biotite is rare in (olivine-) gabbro and norite. In gabbro, ilmenite is the main opaque mineral while rutile may be found as inclusion in pyroxene. Magmatic rocks are generally medium-grained and show a variably strong fabric defined by the shape-preferred orientation of euhedral to subhedral and elongated plagioclase, pyroxene and amphibole (Fig. 4ab). This E−W fabric is usually steeply dipping to the North or to the South (Fig. 3). The absence of solid-state deformation (dynamic recrystallization) indicates that the mineral fabric is of magmatic origin. Close to the Jurassic Eita extensional shear zone (Mohn et al. 2012), magmatic foliations are overprinted by greenschist facies deformation.

Diorites and granodiorite in the BZ show a hypidiomorphic structure and are composed of euhedral to subhedral plagioclase and green-brown hornblende. Plagioclase is zoned with a labradorite core and an andesine rim. Hornblende may contain inclusions of clino- and orthopyroxene. Interstitial quartz is frequent. Opaque minerals are mostly ilmenite. In the absence of sub-solidus deformation, rocks in the BZ locally show a preferred orientation of magmatic minerals. They define a magmatic foliation roughly parallel to the

pluton margin and to the S3 foliation in the contact aureole, lying in places at a high angle with respect to the steeply dipping magmatic fabric observed in the CZ (Fig. 3).

Across the pluton, late-stage magma accumulation forms patchy pockets with no apparent foliation (Fig. 4a). These pockets as well as syn-magmatic mafic dykes cross cut the weakly to well foliated gabbro, locally with a sharp contact. Both usually display weakly-foliated pegmatitic textures with up to 5 cm long subhedral plagioclase and poikilitic hornblende crystals that locally include clinopyroxene. In the BZ, mingling between leucocratic and more mafic magma is indicated by pillow structures with chilled margins (Fig. 4c).

In the entire pluton, the amount of garnet, biotite and rare cordierite in magmatic rocks increases towards the contact with metasedimentary xenoliths (Fig. 4d). This trend is combined with a decrease in the modal amount of amphibole and pyroxene. In some places, centimeter-scale veins form massive garnet-rich mafic rocks along contacts with xenoliths. In such rocks, garnet is typically euhedral, can reach up to 1 cm in diameter and bears numerous plagioclase inclusions. Biotite (1 cm in length) is euhedral and interstitial quartz is frequent.

GEOCHRONOLOGY

In order to constrain the emplacement age of the Sondalo gabbroic complex and the timing of associated contact metamorphism, we performed zircon U–Pb isotopic LA-ICP-MS dating on five samples (location indicated on Fig. 3). Three igneous rock samples (M28B73, GM601 and M1B14) were collected across the pluton. In addition, two samples from the migmatitic metasediments were selected in the contact aureole; one migmatitic paragneiss (BPA 003-12c) and one leucosome (few centimeters in thickness) from the contact aureole (BPA 003-12d).

Zircon U–Pb isotopic measurements and trace element analysis were performed at the Institute of Earth Sciences at the University of Lausanne using a sector field Thermo Scientific Element XR ICP-MS coupled to a NewWave 193nm ArF excimer laser ablation device. Detailed analytical conditions are reported as electronic supplementary material. Spot location was guided by transmitted and reflected light observations as well as backscatter electron (BSE) and cathodoluminescence (CL) images (Fig. 6 and 7). Isotopic ratios and ages are reported as supplementary material and in Fig. 5. Results were plotted in conventional and inverse Concordia diagrams (Figs 6 and 7) using Isoplot/Ex 3.75 (Ludwig 2012) with all errors reported at the 2σ level. For igneous rock and leucosome sample, discordant (concordancy level of 97-103 %) and outlier ages (radiogenic Pb loss, initial Pb incorporation or inherited cores) were discarded for Concordia age calculation. For the migmatitic paragneiss sample, the Discordia line was anchored to an initial Pb ratio of 0.8534 (assumed for an age of 290 Ma following Stacey and Kramers 1975). Outlier ages were discarded for age determination.

Sample description

Magmatic rocks from the gabbroic complex

Diorite M28B73 [46.39551°N; 10.34243°E] was collected about 10 m from a Sil–Bt metapelitic xenolith in the dioritic rim in the northern part of the pluton. It contains Bt–Pl–

Kfs–Qtz with minor garnet, muscovite and ilmenite. The sample is phaneritic (up to 5 mm in size) and preserves its original magmatic texture with weak solid-state deformation attested by discrete undulose extinction in quartz. Plagioclase (andesine) is locally replaced by secondary muscovite and is preferentially oriented along a weakly developed magmatic foliation that, in the field, is steeply dipping to the North. Interstitial biotite (1 mm) contains ilmenite and zircon inclusions and is occasionally chloritized. Zircon is also included in quartz. K-feldspar corresponds to microcline with patchy exsolution lamellae of albite. Tiny garnet (<1 mm in size) contains rare quartz inclusions. At the outcrop scale it becomes more abundant towards the metapelitic xenolith.

Deformed diorite GM601 [46.36016°N; 10.31110°E] was sampled a few meters away from the contact with the overlying Grosina unit in the vicinity (5 m) of the Eita Shear zone, at the south-western margin of the pluton. This deformed diorite is cutting through the metapelitic host rock at a high angle with respect to the S3 foliation of the migmatitic aureole. The magmatic structure is pervasively overprinted by a mylonitic foliation. The sample contains Ms–Bt–Pl–Kfs–Qtz. Porphyroclastic plagioclase and K-feldspar phenocrysts (up to 2.5 mm in size) are dismembered by numerous brittle cracks. Small porphyroclastic muscovite (0.5 mm) recrystallizes into fine-grained muscovite, whereas biotite occurs only as fine-grained aggregates. Quartz is totally recrystallized into fine grains (few μm) by a bulging mechanism, which brackets the deformation temperature between 300 and 400 °C (Stipp et al. 2002), i.e. at greenschist facies conditions. Quartz aggregates occasionally contain zircon grains.

Leucocratic diorite M1B14 [46.34483°N; 10.32495°E] was sampled close to a large roof pendant in the pluton, in contact with very fine-grained gabbro showing a pillow structure and chilled margins. This sample still preserves a magmatic texture with no sub-solidus deformation. It is essentially composed of Pl–Hbl±Kfs. Plagioclase (labradorite, few mm in length) is subhedral while common fine-grained hornblende is interstitial and rare biotite is chloritized. Small garnet (up to 100 μm in diameter) contains inclusions of plagioclase and ilmenite, whereas ilmenite in the matrix is usually associated with hornblende. Quartz bears rare zircon inclusions.

Leucosome and migmatitic paragneiss

Leucosome BPA 003-12d [46.35977°N; 10.33070°E] comes from a metatexite collected in the western part of the contact metamorphic aureole, few tens of meters from the pluton. The rock contains Bt–Grt–Pl–Kfs–Qtz with minor muscovite, sillimanite and ilmenite. The weak shape-preferred orientation of euhedral plagioclase causes a preferential orientation of interstitial biotite, all aligned along S3, without presenting any sub-solidus recrystallization. Biotite is euhedral to subhedral. Atoll to euhedral garnet (up to 3 mm in diameter) is frequent and includes tiny biotite, plagioclase, quartz and ilmenite. Muscovite and partially chloritized biotite form nests with polygonal borders, probably after cordierite. Ilmenite from the matrix contains rare rutile inclusions, whereas zircon is included in biotite. This sample comes from the same outcrop as kinzigite BPA 003-11a for which $P-T$ conditions are estimates at 5.2 kbar at 800 °C (Petri et al. 2016).

Migmatitic paragneiss BPA 003-12c [46.35977°N; 10.33070°E] is a metasedimentary metatexite. It presents alternation of leucosome and melanosome bands (few centimeters in

thickness) parallel to the moderately NW-dipping S3 foliation. The leucosome is composed of Ms–Grt–Crd–Kfs–Qtz±Bt±Sil±Ilm whereas the melanosome includes Grt–Sil–Crd–Bt–Kfs–Qtz±Spl±Pl. Red-brown biotite from the melanosome contains numerous zircon inclusions. Ilmenite is the only opaque phase in the rock. Zircon is included in biotite from the melanosome, and occasionally in quartz from the leucosome. This sample comes from the same outcrop as kinzigite BPA 003-11a (see comment above).

Zircon morphology and internal structure

Zircon grains from magmatic rocks of the gabbroic complex (samples M28B73, GM 601 and M1B14, Fig. 6 a, b and c) are up to 300 μm in length and 100 μm in width. They present elongated shapes, are prismatic, euhedral to sub-euhedral, with slightly rounded outlines. A few grains from sample M1B14 show irregular outlines pointing to late-magmatic chemical corrosion without or with low recrystallization/overgrowth. CL images reveal frequent oscillatory zoning and rare homogenous cores. Zoning is sometimes disrupted and overgrown by a zoned rim. Sub-solidus recrystallization due to late- to post-magmatic processes is attested by heterogeneous patchy patterns (brecciated) or by the presence of thin homogenous and bright rims (up to 10 μm in thickness) or cracks.

Zircon extracted from migmatitic metasediments (samples BPA 003-12d and BPA 003-12c, Fig. 7a and b) are up to 300 μm in length and 100 μm in width for the leucosome BPA 003-12d and up to 200 μm in length and 80 μm in width for the migmatitic paragneiss BPA 003-12c. They are usually elongated and prismatic, with slightly rounded outlines. Cores present a well-developed oscillatory zoning sometimes disrupted by a bright and homogeneous rim (> 10 μm in thickness) penetrating occasionally deeply into the grain (up to 20 μm from the rim for sample BPA 003-12c). Rare xenocrystic cores were observed.

U–Pb dating results

Diorite M28B73 (Fig. 6a): twenty-nine analyses were carried out on twenty-six zircon grains. Most of the analyses are concordant to sub-concordant, the main population ranging between 284 and 302 Ma, with a maximum at *ca.* 292 Ma. A rather homogeneous age population defines a Concordia age of 289 ± 4 Ma (MSWD = 0.22) constrained by thirteen spot analyses. Sub-concordant analyses are slightly marginal with respect to the main population, probably due to younger lead loss. No significant age difference could be observed between zircon textures and analyses location.

Deformed diorite GM601 (Fig. 6b): thirty spot analyses were performed on twenty-five zircons. Analyses of zircon cores point to slightly older ages than rim analyses. The main age population spans between 282 and 298 Ma, with a maximum probability at *ca*. 287 Ma. A homogeneous population of thirteen analyses defines an age of 285 ± 2 Ma (MSWD = 0.33) on a conventional Concordia diagram. The older age population visible on the histogram is mainly composed of discordant ages, probably due to common lead incorporation.

Leucocratic diorite M1B14 (Fig. 6c): nine analyses were performed on eight grains. $^{206}Pb/^{238}U$ ages range from 283 to 291 Ma, with a peak at *ca.* 284 Ma. After discarding discordant and outlier ages, three concordant analyses yields a Concordia age of 285 ± 6 Ma (MSWD = 0.10).

Leucosome BPA 003-12d (Fig. 7a): five spot analyses were carried out on 4 zircon grains. One spot from a zircon core yielded an inherited age of 854 ± 5 Ma. The remaining four spots lies between 282 and 292 Ma showing a poorly constrained peak around 286 Ma. They define a Concordia age of 288 ± 5 Ma (MSWD = 0.037).

Migmatitic paragneiss BPA 003-12c (Fig. 7b): out of four spot analyses performed on 3 zircons, only one is strictly concordant at 288 ± 3 Ma. Three spots lie along a mixing line between initial Pb defining a Discordia line with a lower intercept at 289 ± 4 Ma (MSWD = 0.01) on an inverse Concordia diagram.

U, Th, Hf and trace element geochemistry of zircon

U, Th, Hf and trace element concentrations in zircon were analyzed to constrain the conditions of zircon growth. Raw analytical results and parameters are provided as supplementary material. Parameters are reported in Fig. 8 as well as supplementary material. REE composition diagrams, Eu/Eu* (Eu-anomaly, $Eu_n/((Sm_n+Gd_n)/2)$) and Yb_n/Gd_n (slope of the REE pattern) are normalized to the C1–chondrite composition of Sun & McDonough (1989).

Magmatic rocks from the gabbroic complex

Typically, most magmatic zircons present a steep HREE pattern (Fig. 8ab), with a positive Ce-anomaly, a negative Eu-anomaly, and Th/U ratios > 0.01, characteristic for magmatic zircons (Murali et al. 1983; Schaltegger et al. 1999; Rubatto 2002).

Zircons from sample M28B73 present a relatively high Th/U ratio (0.036–0.338). A decrease of the HREE content (from $Yb_n/Gd_n \approx 40$ to $Yb_n/Gd_n \approx 0$–10) is balanced by a reduction of the Eu-anomaly, with Eu/Eu* varying from 0.023 up to 0.160, with younger zircon domains having a low Yb_n/Gd_n and a high Eu/Eu* values (Fig. 8a). The slope of the HREE diagram is inversely correlated to the Nb/Ta ratio due to a decreasing Ta content while Yb_n/Gd_n decrease and Nb/Ta increase (Fig. 8a). Similarly, Hf and U-contents weakly decrease with lower Yb_n/Gd_n values (see supplementary material).

A high Th/U ratio (0.137–0.597) is found for zircons of sample M1B14 (Fig. 8b). They present a relatively low HREE-enrichment ($Yb_n/Gd_n < 20$) and a negative Eu-anomaly (Eu/Eu* = 0.063–0.240). No clear trend between Yb_n/Gd_n or Eu/Eu* is observed. Zircons commonly have a low Ta concentration (around 0.8 ppm) that is not correlated with the Nb/Ta ratio (see supplementary material). Similarly, they are poor in Hf and U, with around 9000 and 600 ppm, respectively. Both element concentrations do not present any peculiar correlation with Yb_n/Gd_n (see supplementary material).

Leucosome and migmatitic paragneiss

Metasediments sampled in the contact aureole (leucosome BPA 003-12d and migmatitic paragneiss BPA 003-12c, Fig. 8c) present a homogeneous REE pattern, with the exception of inherited cores. They have a high Th/U ratio (0.194–0.624), are depleted in HREE ($Yb_n/Gd_n \approx 2$) and present a medium Eu-anomaly (Eu/Eu* ≈ 0.14, Fig. 8c). The Ta-content commonly varies between 0.9 and 4.0 ppm without being correlated to the Yb_n/Gd_n and Nb/Ta ratios (Fig. 8c). The Hf and U concentration in zircon is weakly but inversely correlated to the Yb_n/Gd_n ratio (see supplementary material).

DISCUSSION

Significance of zircon chemistry and interpretation of U–Pb ages

Magmatic rocks from the gabbroic complex

U–Pb zircon ages on magmatic zircons from the Sondalo gabbroic complex are similar within error, ranging from *ca.* 289 ± 4 Ma to 285 ± 6 Ma. These results are in line with previous Sm–Nd dating of 300 ± 12 and 280 ± 10 Ma (Tribuzio et al. 1999) and older than the U–Pb zircon age of 270 Ma (Bachmann and Grauert 1981).

The oldest concordant age in magmatic rocks is found in a diorite sample (M28B73) at *ca.* 289 ± 4 Ma. Notably, most of the oldest zircon grains from this sample display steep slopes of HREE and high negative Eu-anomalies, which may indicate the initial crystallization of a garnet-free magma associated with well crystallized plagioclase (Rubatto, 2002). In contrast, the reduction of the negative Eu-anomaly in younger zircon grains (Fig. 8a) indicates a mixing with a less evolved liquid where plagioclase had not completely crystallized. The associated lower Yb_n/Gd_n values point to a progressive depletion of the residual liquid, generally interpreted as reflecting a progressive crystallization of garnet (Rubatto, 2002), a mineral which is observed in the sample. Ilmenite and biotite are the main hosts for Nb and Ta, but biotite preferentially incorporates Nb over Ta, in contrast to ilmenite (Xiong et al. 2011; Stepanov and Hermann 2013; Galster 2015). The Nb/Ta ratio is inversely correlated to the Ta content while the Ta content decreases with decreasing Yb_n/Gd_n (see supplementary material). This indicates that magmatic ilmenite (or a precursor rutile) is the main phase that fractionates Nb over Ta during crystallization of zircon and before crystallization of magmatic biotite (Galster 2015). This is in agreement with the presence of zircon grains included in interstitial biotite. The weak decrease of Hf content (see supplementary material) is not consistent with its expected increase during magmatic differentiation (Linnen and Keppler 2002; Hoskin and Schaltegger 2003). This may be explained by the crystallization of magmatic ilmenite synchronously with zircon crystallization, during or after the crystallization of plagioclase.

Field observations point to increasing garnet, biotite and cordierite contents in magmatic rocks towards the metapelitic xenoliths (Fig. 4d), indicating progressive magma hybridization with melts derived from partially molten metapelites. This scenario may explain the crustal assimilation signature of isotopic data (ε_{Nd} and $^{87}Sr/^{86}Sr$; Tribuzio et al. 1999). Zircon trace element chemistry of diorite sample M28B73, with decreasing Yb_n/Gd_n, is coherent with the presence of garnet in the rock, a phase generally enriched in HREE. In the absence of magma mingling structures close to this sample, it is proposed that the mafic magma was contaminated by the liquid derived from the partially molten metapelites. In such case, a progressive enrichment in LREE, Hf and U is expected in the residual liquid and therefore in zircon. The decreasing Hf and U contents (see supplementary material) may be due to the lack of consumption of Hf and U-rich phases, respectively biotite and zircon, apatite and xenotime in migmatites of the BZ, i.e. where the diorite sample was collected. The residual liquid might be progressively depleted in Hf during the crystallization of magmatic ilmenite. Alternatively, magma contamination is recorded in trace element compositions of gabbros and Ol-gabbros from the CZ (Tribuzio et al. 1999).

The slightly younger concordant ages of the two diorites sampled at the western margin of the pluton lie at 285 ± 2 Ma and 285 ± 6 Ma. The moderately steep to flat HREE profiles (low Yb_n/Gd_n values) combined with strong to moderate negative Eu-anomalies indicate that zircons crystallized in the presence of garnet and plagioclase. The apparently increasing Hf concentration in zircon indicates fractionation during crystallization (Linnen and Keppler 2002; Hoskin and Schaltegger 2003).

Leucosome and migmatitic paragneiss

Leucosome and migmatitic paragneiss samples collected at the same outcrop have similar characteristics. The concordant age of 288 ± 4 Ma for leucosome sample BPA 003-12d is similar (within error) to the lower intercept age of 289 ± 4 Ma in the migmatitic paragneiss (BPA 003-12c). The very low Yb_n/Gd_n coupled to a moderate negative Eu-anomaly attests the presence of garnet and plagioclase during the crystallization of zircon in both samples. The commonly low U value indicates that partial melting of the metapelites did not reach the biotite-out reaction (almost synchronous to apatite and xenotime-out reaction; Bea and Montero 1999) and/or extensive zircon dissolution. This is in agreement with the observed Sil–Bt assemblage in residual parts of the migmatitic metasediments, and the presence of inherited zircon cores (e.g. B4 z10 of sample BPA 003-12d).

Interpretation of U–Pb ages

In conclusion, ages from both magmatic and metamorphic rocks are similar within error, ranging between 289 ± 4 and 285 ± 6 Ma. Zircon chemistry indicates that in plutonic rocks, zircon crystallizes after plagioclase (presence of negative Eu-anomalies). Thus, U–Pb ages record the final crystallization of the magmatic melt in the gabbroic complex and in the migmatitic contact aureole. They do not date older processes associated with magma ascent or younger, post-emplacement alteration. The similar U–Pb ages of the magmatic rocks and the migmatitic metasediments emphasize that the observed partial melting was effectively caused by the emplacement of the Sondalo gabbroic complex in the Campo metasediments. It is also important to note that the age of the deformed diorite (GM601), sampled from a dyke cross-cutting at high angle S3-bearing metasediments, indicates that the S3 foliation has to be older than 285 ± 2 Ma.

The Sondalo intrusion in the Variscan to post-Variscan history of the Austroalpine domain

Variscan evolution

The Campo unit records a pre-Permian prograde metamorphism reaching amphibolite to upper-amphibolite facies (Petri et al. 2016), in agreement with other units from the Austroalpine domain such as the Err, Bernina (Halmes 1991; Büchi 1994) and the Margna units (Guntli and Liniger 1989). We suggest that the yet undated pre-Permian history of the Campo unit is likely Variscan as: (1) the Campo metasediments documents Ordovician protolith ages (U–Pb on detrital zircons; Bergomi and Boriani 2012), (2) Variscan magmatism is documented in the neighbouring Bernina unit (Von Quadt et al. 1994), (3) Austroalpine nappes largely document Variscan cooling ages (see below; Thöni 1981) and (4) adjacent

units shared a similar evolution during Variscan deformation (Hoinkes and Thöni 1993). Indeed, this Variscan prograde metamorphism is dated in the adjacent Ulten area (the Upper Tonale unit) as Lower Carboniferous (351-343 Ma by U–Pb on monazite included in garnet; Langone et al. 2011). Similarly, we correlate the D1 deformation phase in the Campo unit with Variscan crustal thickening during the Lower Carboniferous (Fig. 9a). It was followed by the subsequent D2 deformation stage during the regional thermal peak, estimated to be Middle Carboniferous in the Ulten zone (330-326 Ma by U–Pb on matrix monazite; Langone et al. 2011). This evolution is fairly consistent with the Variscan history documented elsewhere in the Alpine domain (Schaltegger and Gebauer 1999).

Late- to post-Variscan evolution

Decompression of the Campo unit to $P < 4.5$ kbar occurred after the Carboniferous burial and exhumation but before the onset of HT-metamorphism related to the emplacement of the Sondalo gabbroic complex at *ca.* 289–285 Ma. This is indicated by paragenetic relations far from the intrusion, where HT assemblages developed at lower pressure than peak Variscan conditions (see geological setting and discussion in Petri et al. 2016). However, no evidence of retrograde deformation related to this event could be found in the Campo unit. Therefore, we suggest that the Campo unit was tectonically unroofed during the late-Carboniferous/Permian by shear zones structurally higher in the crust before the emplacement of the Sondalo gabbroic complex (Fig. 9b). These shear zones are possibly located in the overlying Grosina unit where undated deformations are observed. This evolution is comparable to the Late Carboniferous history of the Austroalpine domain characterized by a late-orogenic extensional phase associated with exhumation occurring between 310 and 290 Ma. Such an exhumation is evidenced in the Bernina unit where alkaline intrusive rocks emplaced at $P < 3$ kbar and *ca.* 295 Ma are covered by alkaline rhyolites dated at *ca.* 288 Ma (Büchi 1987; Spillmann and Büchi 1993; Von Quadt et al. 1994). Accordingly, cooling of basement rocks in the Silvretta unit ranges between 330 and 310 Ma for K–Ar on micas (Flisch 1986) and *ca.* 310 Ma for Rb–Sr on micas (Thöni 1981).

From 290 to 270 Ma, the Permian post-Variscan extension is interpreted as characterized by a shallow lithosphere-asthenosphere boundary, responsible for the mantle partial melting and associated emplacement of mafic intrusions at all crustal levels (Fig. 9c; McCarthy and Müntener 2015) during crustal extension. In the Austroalpine domain mafic intrusions are emplaced at the crust-mantle boundary and in the lower crust (e.g. the Braccia gabbro; Hermann et al. 1997) as well as in the middle crust (Tribuzio et al. 1999; Braga et al. 2001; this study). In the Campo unit, near-isobaric heating due to contact metamorphism occurred at 5.2–6 kbar during a *P–T* loop that was distinct from the Variscan one (Fig. 1c; Petri et al. 2016). Consequently, from the available pressure and temperature data as well as related deformation history, the Variscan orogenic collapse and the Permian thermal event seems to be, at least locally, two distinct events.

In the Austroalpine domain, the Permian granulite facies metamorphism, and therefore the Permian HT-phase ended at *ca.* 260 Ma (Fig. 9d; Hermann and Rubatto 2003). This event was followed by the onset of subsidence and the deposition of a thick Triassic succession (> 1 km) passing from fluvial to shallow marine conditions (Dössegger et al. 1982; Furrer 1993). The deposition of these sediments is interpreted as related to the thermal re-equilibration post-

dating the Permian HT event and possibly to tectonic and thermal subsidence in relation with Triassic rifting in the Eastern Adriatic domain (Schuster and Stüwe 2008). Geochronological arguments combined with field relationships throughout the Alps indicate that significant exhumation of middle to lower crustal rocks affected by the Permian HT metamorphism occurred only during Jurassic rifting (Villa et al. 2000; Mohn et al. 2012; Galster et al., submitted).

Geodynamic implications

The Sondalo gabbroic complex is one example of a suite of intrusive bodies that testify the occurrence of an important magmatic and metamorphic Permian event documented across whole Western Europe.

Intra-continental basins filled by volcano-sedimentary sequences are widespread across the former Variscan realm. Some of them were already opened during the Carboniferous (Fig. 10; Capuzzo and Wetzel 2004; Cassinis and Perotti 2007). This attests for a topographic attenuation and a re-equilibration of the crustal thickness during the Late Carboniferous to Permian (Lorenz and Nicholls 1984; Burg et al. 1994) in an extensional to transtensional tectonic regime (Henk 1999).

An increasing number of studies presents strong evidences for a Permian magmatic and metamorphic event that can be observed throughout large parts of Western Europe. In the Alpine belt, a thinning of the lithosphere is attested by the isotopic signature of mantle rocks indicating Permian partial melting (Rampone et al. 1998; Müntener et al. 2004; McCarthy and Müntener 2015), accretion of underplated magmatic bodies (Voshage et al. 1987; Libourel 1988; Vielzeuf and Pin 1991; Hermann et al. 1997) and mid- to upper-crustal mafic intrusion (Tribuzio et al. 1999; Monjoie et al. 2007; Tribuzio et al. 2009; Petri et al. 2016). Synchronously, the lithospheric thinning combined with widespread mafic magmatism was responsible for HT metamorphism ranging from greenschist to granulite facies (Schuster and Stüwe 2008). Indeed, in the Alps but also in Calabria, in Corsica and in the Pyrenees, most of the high-grade rocks are associated in the field to mafic plutons emplaced at the same pressure conditions (Figs 10 and 11; Vielzeuf 1984; Libourel 1985; Lardeaux and Spalla 1991; Barboza and Bergantz 2000; Müntener et al. 2000; Braga et al. 2001; Caggianelli et al. 2007). In addition to mafic magmatism, felsic intrusives and extrusives were emplaced at shallower crustal levels in the Alps (e.g. Von Quadt et al. 1994; Galli et al. 2012), but also elsewhere such as in Sardinia (e.g. Cortesogno et al. 1998) and in the Pyrenees (see Denèle et al. 2012 and references therein). Based on both geochronological and geochemical arguments (e.g. Marquer et al. 1998; Schaltegger and Brack 2007), part of this felsic magmatism originated from mafic intrusives by a combination of magmatic differentiation and mixing with crustal-derived melts (e.g. Sinigoi et al. 2016). However, evidence for Permian underplated gabbros and HT-metamorphism are not restricted to domains that underwent Mesozoic rifting only. Lower crustal xenoliths in Tertiary to Quaternary lavas are also exhuming mafic magmatic rocks in the French Massif Central ($\geq$ 257 Ma; see references in caption of Fig. 10) as well as felsic granulites (not always associated to mafic rocks; Fig. 11) in the Spanish Central System (*ca.* 312-277 Ma) and in the French Massif Central (*ca.* 300-280 Ma). However, available ages indicate that mafic magmatism is slightly older in the Pyrenees (*ca.* 312-293 Ma) and is

progressively younging towards Calabria (*ca.* 298-295 Ma), Corsica (*ca.* 289-280 Ma) and across the Alps (*ca.* 290-280 Ma).

Mafic intrusions seem to emplace in segments of the Variscan chain that were still in compression in the Pyrenees (hence syn- to late-Variscan; Aguilar et al. 2014; Aguilar et al. 2015). However, several lines of evidence question the direct relationship between the collapse and the partial melting of the mantle: (1) the main mafic magmatic activity post-dates the crustal re-equilibration in some places (Ivrea zone, Barboza et al. 1999; Campo unit, Petri et al. 2016); (2) the depth of emplacement of Permian pluton do not exceed 11 kbar (Spalla et al. 2014); (3) Permian HT-metamorphism is also limited to 11 kbar (e.g. Galli et al. 2010; Manzotti and Zucali 2013; Redler et al. 2013; Spalla et al. 2014); (4) the Permian magmatic system is not restricted to the former orogenic domain (e.g. Northern Germany; Timmerman 2004; Wilson et al. 2004) and finally (5) tectonic extension due to plate divergence is needed to explain the amount of extension in intra-continental Permian basins in the former orogenic domain (Henk 1999). Whereas it cannot be excluded for all segments of the Variscan orogeny, the Permian event is not clearly associated with the collapse of the Variscan orogeny. We therefore suggest that the main phase of Late- to Post-Variscan crustal thinning occurred in Late Carboniferous followed during the Permian by an important thinning of the lithospheric mantle while the continental crust was already equilibrated at *ca.* 30–35 km. Synchronous extension and addition of large volumes of mantle-derived melts may have maintain the crustal thickness to *ca.* 30–35 km (e.g. Thybo and Artemieva 2013), despite lithospheric and crustal extension during the Permian and hence postponing the marine transgression to Triassic time.

CONCLUSIONS

The following conclusions can be drawn from our study:

1. The intrusion of the Sondalo gabbroic complex caused partial melting of the host rock Campo unit by contact metamorphism. U–Pb on zircon ages from magmatic and metamorphic rocks are similar and are ranging between 289 ± 4 and 285 ± 6 Ma.
2. Trace element geochemistry of zircons from magmatic rocks points to an initial crystallization of zircon in absence of garnet and with plagioclase already crystallized (steep HREE slopes and high Eu-anomalies), progressively mixed with a less evolved liquid with plagioclase not completely crystallized and an increasing garnet content (decreasing HREE slopes and decreasing Eu-anomalies). This second melt infiltration is probably derived from the surrounding partially molten metapelites.
3. The Austroalpine units preserve a complex late- to post-Variscan history. From 310 to 290 Ma, late-orogenic extension is associated with emplacement of calc-alkaline to alkaline magmas and exhumation of orogenic crustal units. From 290 to 260 Ma, post-orogenic extension is associated with a shallow lithosphere-asthenosphere boundary, responsible for synchronous emplacement of mafic magmas and associated HT-metamorphism. After ~260 Ma, the HT Permian conditions decay, followed by thermal re-equilibration and the deposition of Middle to Upper Triassic fluvial to shallow-marine sediments.
4. We suggest that this Permian event occurred after the termination of post-Variscan crustal reequilibration (i.e. the collapse). Consequently, the Permian mafic

magmatism seems to post-date the Variscan collapse in the Austroalpine domain, and probably in Western Europe, although such processes may vary in time and space.

ACKNOWLEDGMENTS

B. Petri was supported by the University of Strasbourg. Fieldwork and analysis were financed by an ExxonMobil research grant to G. Manatschal. R. van Elsas and A. Aubert are thanked for the help with mineral separation, and P. Vonlanthen and G. Morvan for the BSE and CL imaging, A. Ulianov for the help with the LA-ICP-MS. A. Bouzeghaia is warmly thanked for her help with figures. O. Müntener is thanked for discussions. All authors acknowledge careful reviews from N. Froitzheim and A. Galli and W.-C. Dullo for editorial handling.

COMPLIANCE WITH ETHICAL STANDARDS

Funding: Field work and analyses have been financed by an ExxonMobil research grant to G. Manatschal.

Conflict of Interest: The authors declare that they have no conflict of interest.

ELECTRONIC SUPPLEMENTARY MATERIAL

ESM 1 Geochronological methods

ESM 2 U–Pb isotopic data for zircon from magmatic samples (diorites) analysed by LA-ICP-MS

ESM 3 U–Pb isotopic data for zircon from metamorphic samples (leucosome and migmatitic paragneiss) analysed by LA-ICP-MS

ESM 4 U, Th and trace element (REE) concentration of zircon from magmatic samples (diorites) analysed by LA-ICP-MS

ESM 5 U, Th and trace element (REE) concentration of zircon from metamorphic samples (leucosome and migmatitic paragneiss) analyzed by LA-ICP-MS

ESM 6 REE and trace element compositional diagrams for diorite M28B79, diorite M1B14 and for metasediments (leucosome and migmatitic paragneiss)

FIGURE CAPTIONS

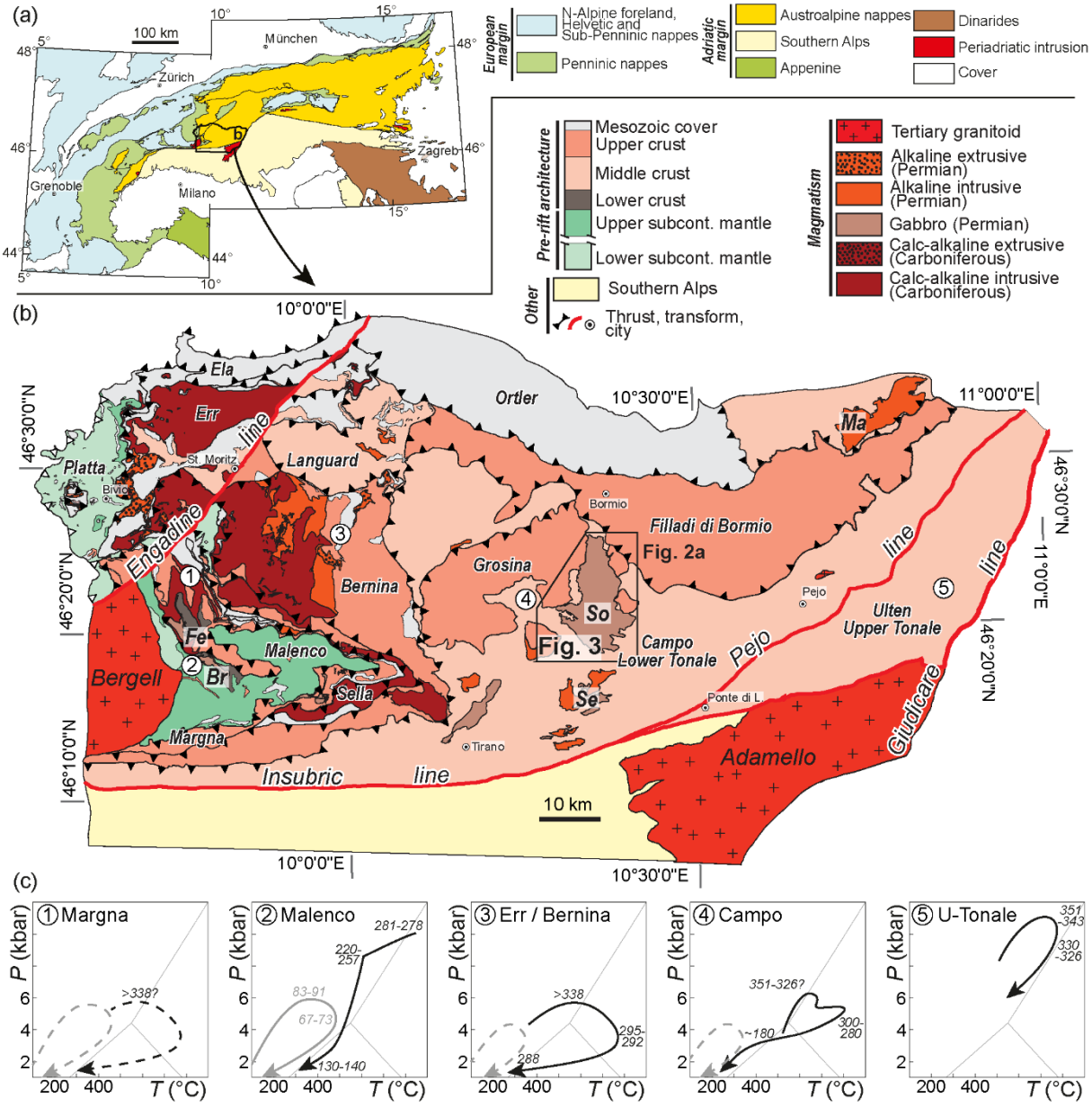

Fig. 1: (a) Tectonic map of the Alps, modified after Schmid et al. (2004). (b) Litho-tectonic map of the Austroalpine domain in SE Switzerland and N Italy representing the different pre-rift crustal levels. The map is a compilation of Del Moro & Notarpietro (1987), Del Moro et al. (1999), Gosso et al. (2004), Mohn et al. (2011), Staub (1946), the 1:25,000 geological maps of Switzerland, the 1:10,000 and 1:25,000 geological maps of Italy and personal observations. Black rectangle in (b) reports location of the map in Fig. 3. Main Permian intrusives are reported and correspond to Fe, Fedoz gabbro; Br; Braccia gabbro; So, Sondalo gabbro; Se, Serottini intrusives; and Ma, Martell granite. Pre-Carboniferous intrusives are not depicted. (c) Reconstructed *P–T–t* paths for different Austroalpine units. Black arrows represent the pre-Alpine evolution, grey arrows the Alpine evolution. *P–T–t* paths are from (1) Guntli and Liniger (1989), (2) Müntener et al. (2000) and Villa et al. (2000), (3) Spillmann and Büchi (1993) and Von Quadt et al. (1994), (4) Petri et al. (2016) and (5) Langone et al. (2011). See text for details

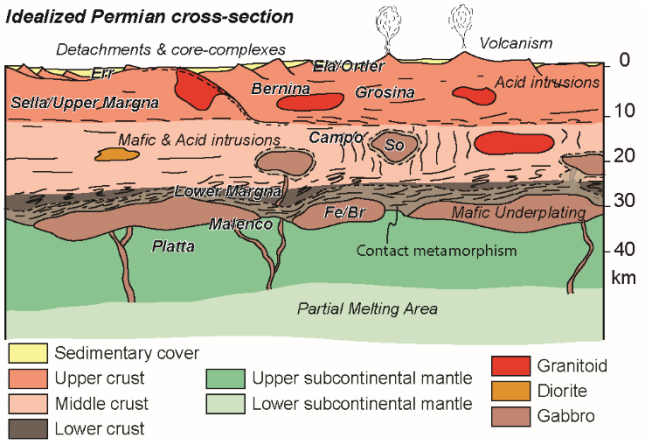

Fig. 2: Schematic cross-section of the lithosphere in the Permian in the Austroalpine domain. “Fe” stands for the Fedoz gabbro, “Br” for the Braccia gabbro and “So” for the Sondalo gabbro. Modified after Mohn et al. (2012) and Galli et al. (2012)

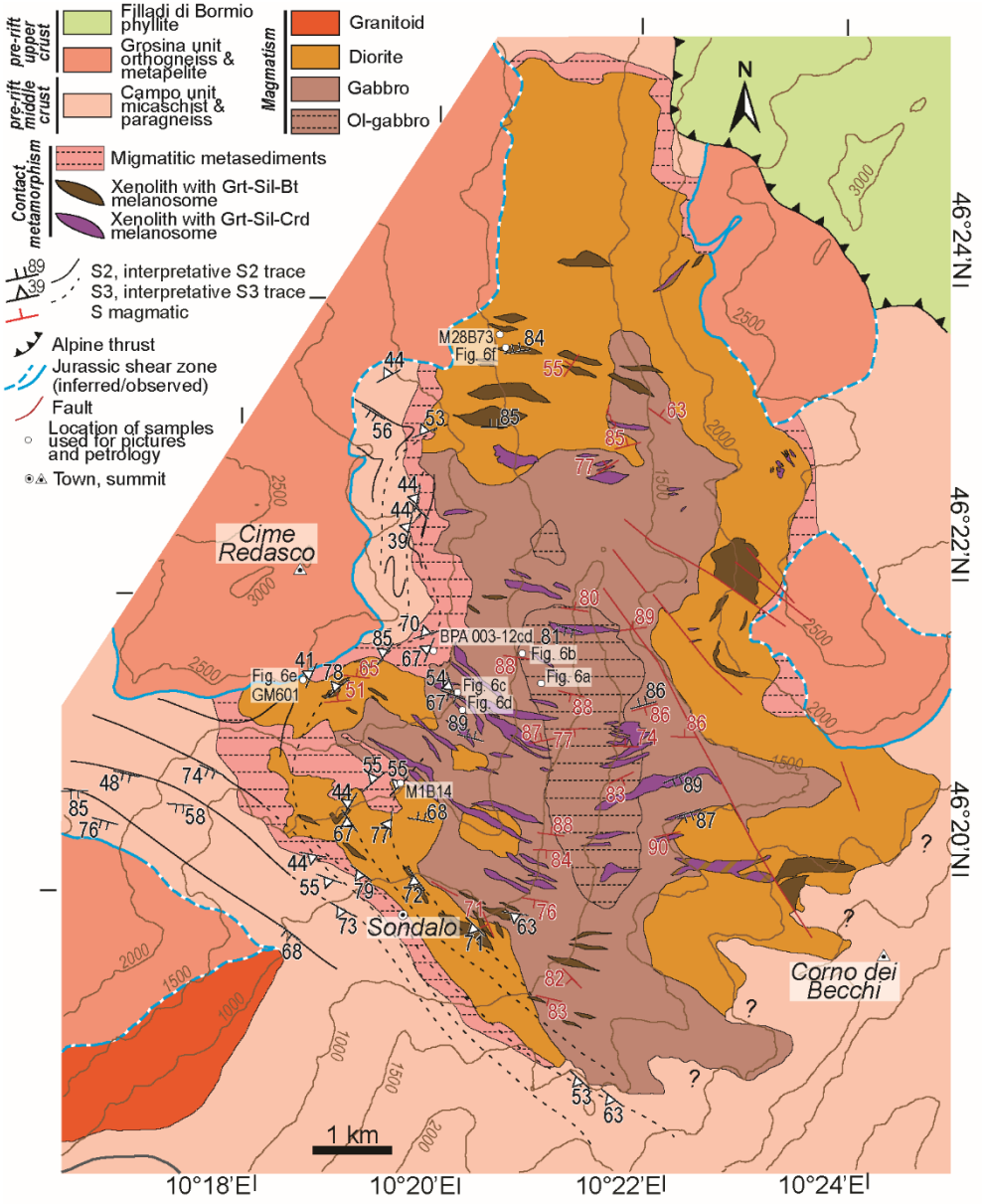

Fig. 3: (a) Geological and structural map of the Sondalo gabbroic complex and the host rock Campo unit. Location of field photographs (Fig. 4) and samples used for geochronology is indicated. Contour interval is 500 m

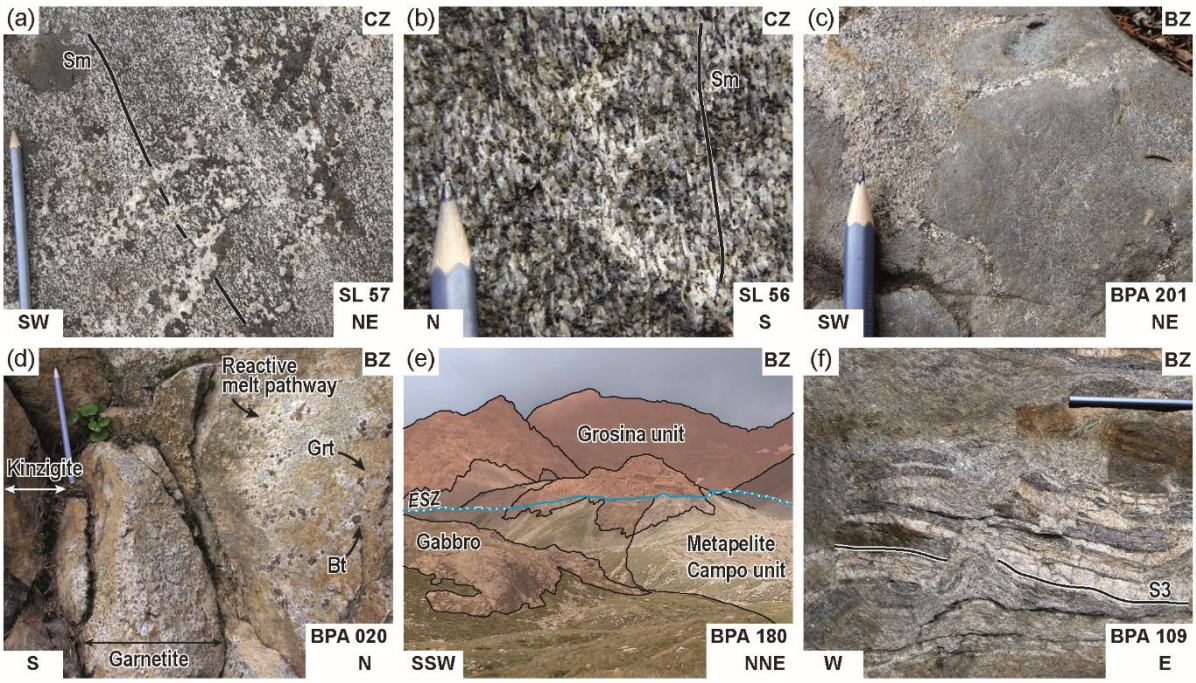

Fig. 4: Field photographs of mafic rocks. (a) Patchy pegmatites due to late-stage accumulation of interstitial liquid. Note the modal lamination of the fine-grained and foliated gabbro. (b) Strong foliation defined by shape-preferred orientation of plagioclase and amphibole. (c) Magma mingling with chilled mafic magma in contact with a leucocratic diorite. (d) Magmatic rocks around a kinzigitic xenolith. Note the formation of garnet-rich mafic rock at the contact and the presence of small-scale reactive melt pathways with formation of large euhedral biotite and garnet (up to 2 cm in width). (e) Panoramic view on the contact aureole below the Grosina unit separated from the Campo unit by the Eita Shear Zone (ESZ). (f) Metapelitic migmatite from a xenolith surrounded by diorite. Location of photographs is indicated on Fig. 3, "CZ" stands for Central Zone and "BZ" for Border Zone

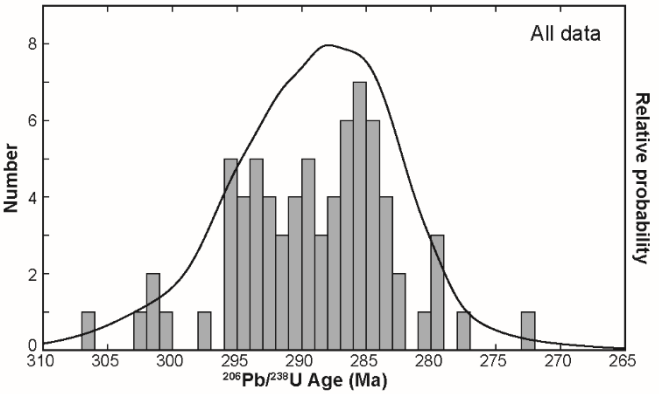

Fig. 5: Histogram and relative probability plots of single-spot $^{206}Pb/^{238}U$ ages on zircon from diorites, leucosome and migmatitic paragneiss and individual uncertainties

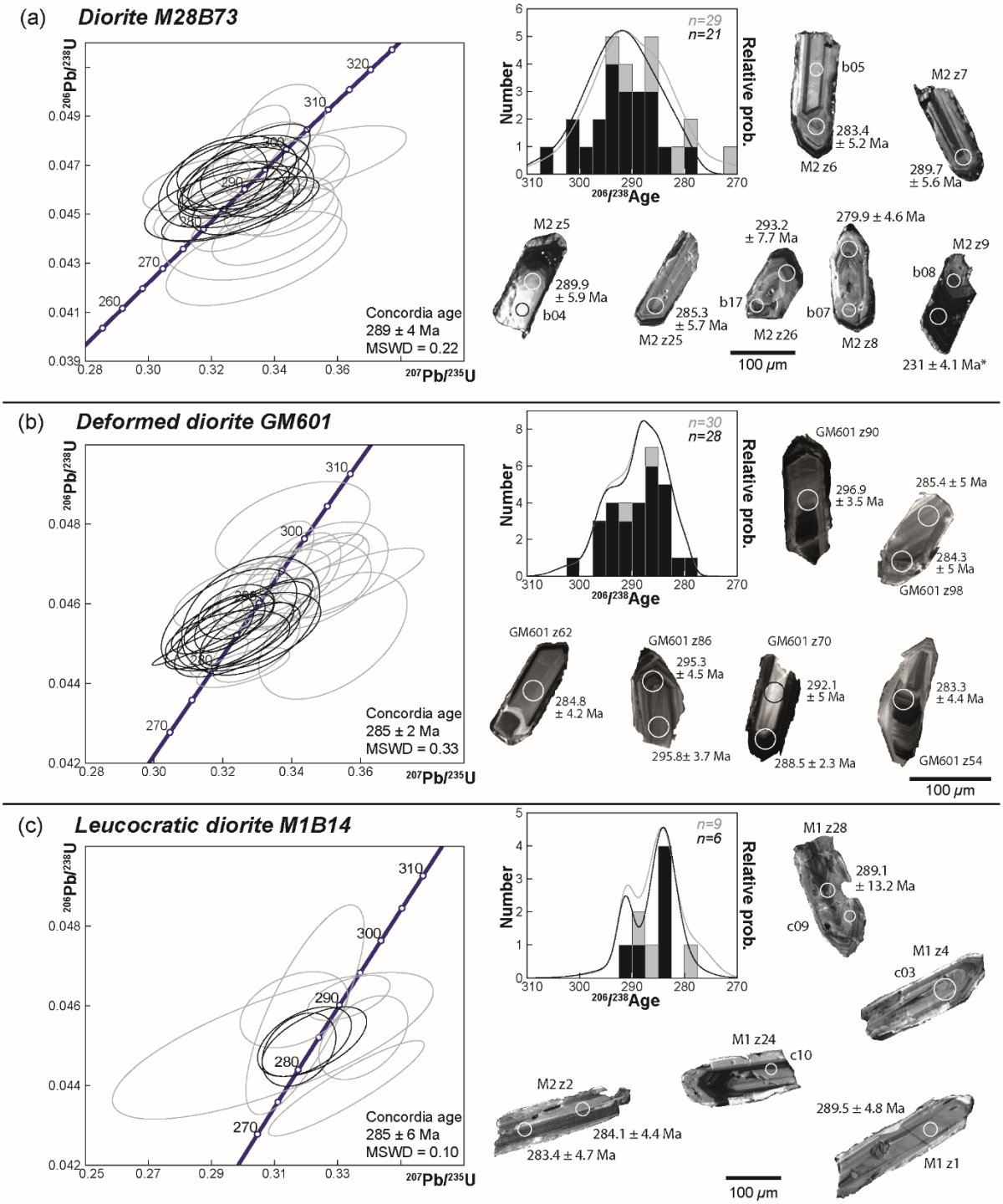

Fig. 6: Conventional Concordia age diagrams of U–Pb ages on zircon from LA-ICP-MS analyses performed on diorites, histograms of single-spot $^{206}Pb/^{238}U$ ages (grey: all data; black: concordant data) and CL images of zircons for diorites (a) M28B73, (b) GM601 and (c) M1B14. Concordia diagrams were calculated using Isoplot/Ex 3.75 (Ludwig 2012), grey ellipses were not used for age calculation, ellipses are plotted at 95% level of confidence and age errors are reported at a 2σ level. Spot location for U–Pb and trace element analyses are indicated along with $^{206}Pb/^{238}U$ ages. * indicates discordant ages

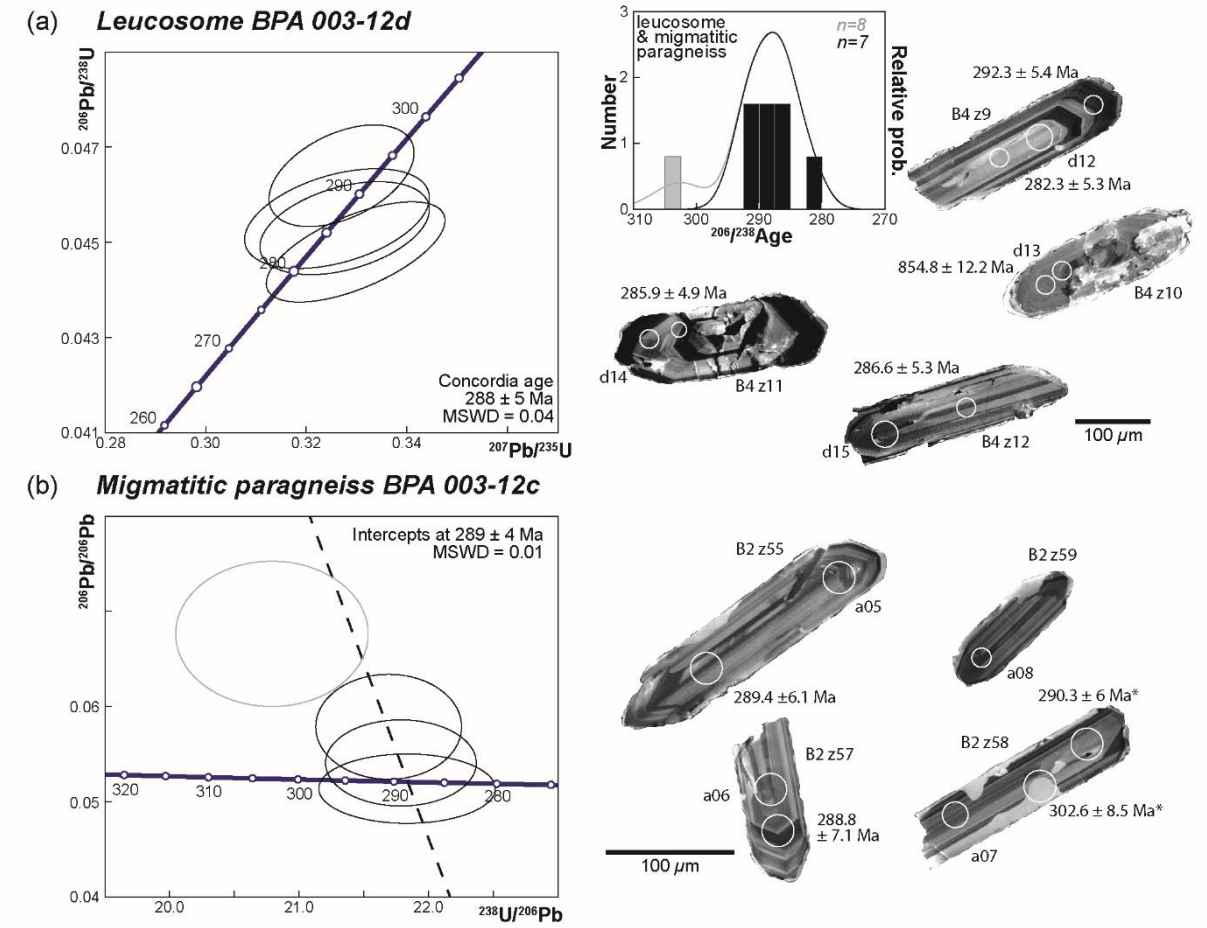

Fig. 7: Conventional and inverse Concordia age diagrams of U–Pb ages on zircon from LA-ICP-MS analyses performed on migmatitic metasediments, histograms of single-spot $^{206}Pb/^{238}U$ ages (grey: all data; black: concordant data) and CL images of zircons for (a) leucosome BPA 003-12d and (b) migmatitic paragneiss BPA 003-12c. Concordia diagrams were calculated using Isoplot/Ex 3.75 (Ludwig 2012), grey ellipses were not used for age calculation, ellipses are plotted at 95% level of confidence and age error are reported at a 2σ level. Spot location for U–Pb and trace element analyses are indicated along with $^{206}Pb/^{238}U$ ages. * indicates discordant ages

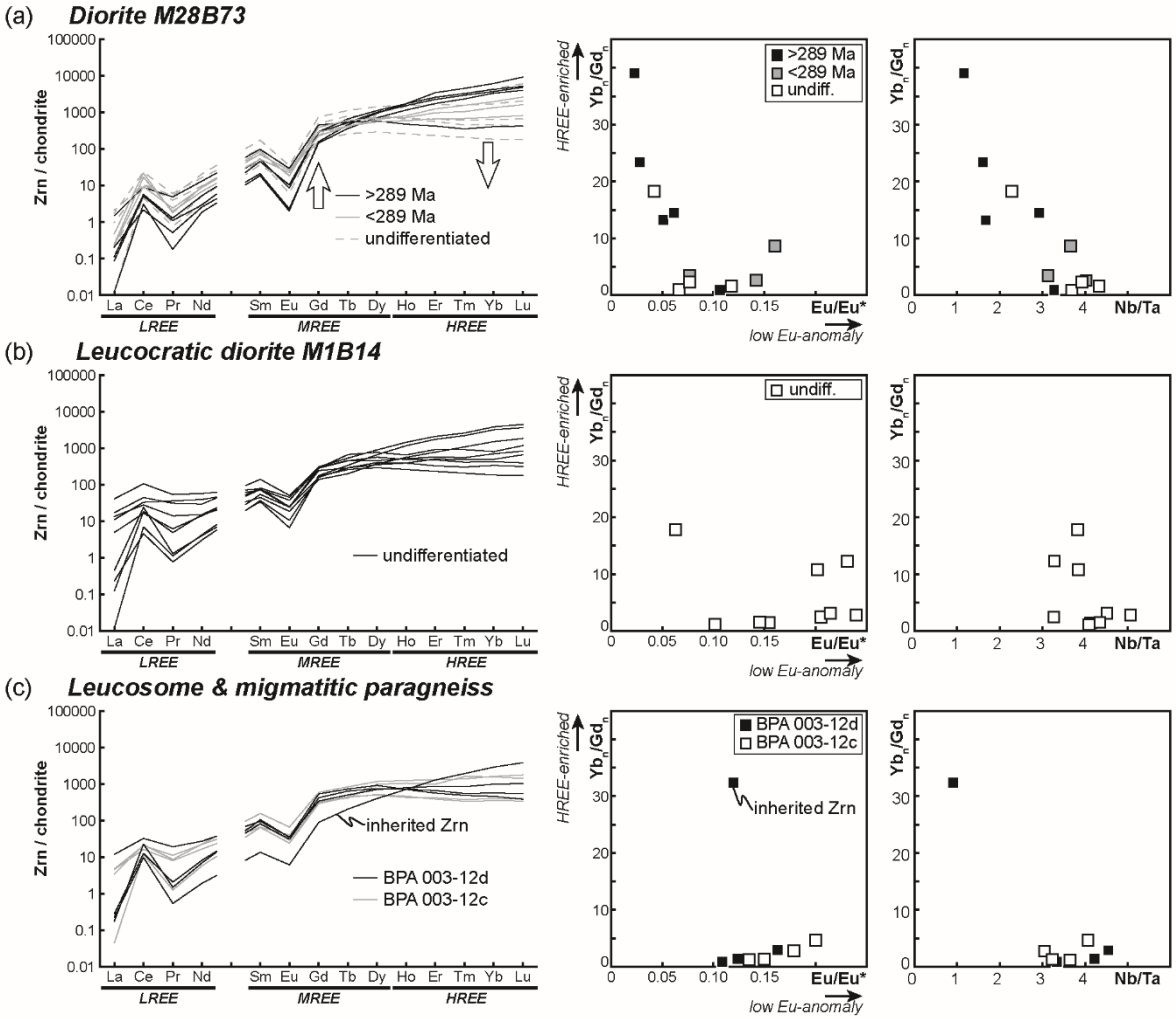

Fig. 8: REE and trace element patterns and compositional diagrams for (a) diorite M28B79, (b) diorite M1B14 and (c) for metasediments (leucosome and migmatitic paragneiss). Spot locations are indicated on Figs 6 and 7. REE compositions and ratios are normalized to the C1–chrondrite composition of Sun and McDonough (1989)

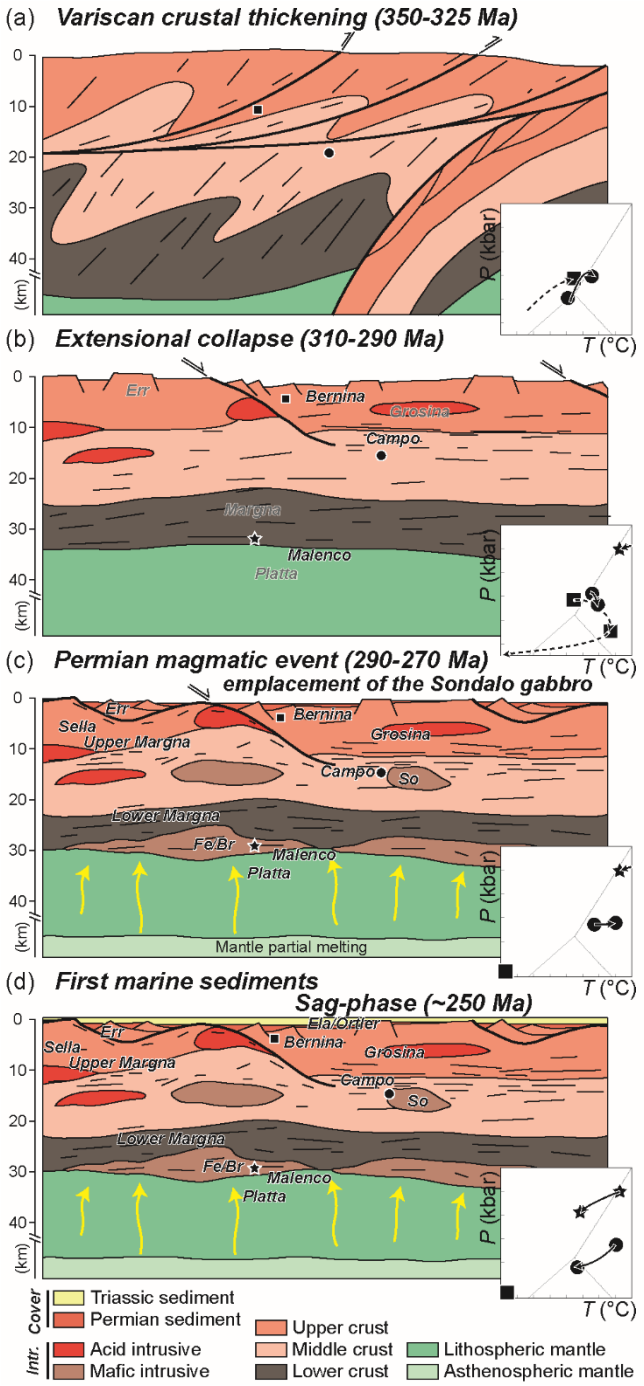

Fig. 9: Schematic tectonic evolution of the Austroalpine domain during (a) Variscan orogeny (350–325 Ma), (b) Extensional collapse of the Variscan orogeny (310–290 Ma), (c) the Permian magmatic event (290–270 Ma) and (d) post-tectonic cooling of the lithosphere. See text for detailed explanations. “Fe”, “Br” and “So” refer to the Fedoz, the Braccia and the Sondalo gabbro, respectively. *P–T* data are compiled from Spillmann and Büchi (1993), Müntener et al. (2000) and Petri et al. (2016). The position of different Austroalpine units is indicated (in transparency when poorly constrained)

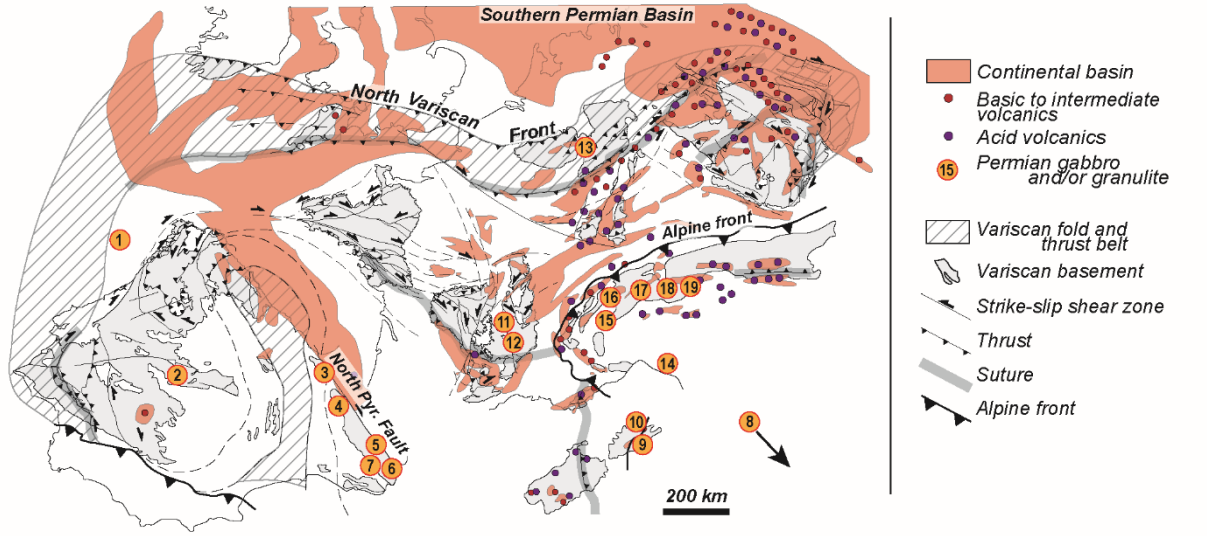

Fig. 10: Maps of Early Permian (Autunian, 290–260 Ma) sedimentary basins and volcanics compiled from Trümpy and Dösseger (1972), Lorenz and Nicholls(1976) , Feys (1989), Châteauneuf (1989), Burg et al. (1994) and Cassinis et al. (2012). Late Carboniferous and Early Permian gabbros and granulites exhumed by tectonic activity or Tertiary to Quaternary volcanoes are indicated with: 1 – Iberian margin (ODP Site 1069; Manatschal et al. 2001); 2 – Spanish Central System (Fernández-Suárez et al. 2006; Villaseca et al. 2007); 3 – Gavarnie-Héas dome (Kilzi et al. 2016);4 – Ursuya massif, Pyrenees (Vielzeuf 1984; Vielzeuf and Kornprobst 1984); 5 – Quérigut massif, Pyrenees (Roberts et al. 2000); 6 –Treilles norite, Pyrenees (Vielzeuf and Pin 1991); 7 – Ceret gabbro, Pyrenees (Aguilar et al. 2014); 8 – Calabria (Schenk 1980; Caggianelli et al. 2013); 9 – Santa Lucia massif, Corsica (Paquette et al. 2003; Rossi et al. 2006); 10 – Bocca di Tenda gabbro, Corsica (Cocherie et al. 2005; Tribuzio et al. 2009); 11 – Puy Beaunit, French Massif Central (Downes et al. 1991; Costa and Rey 1995; Féménias et al. 2003); 12 – Bournac, French Massif Central (Rossi et al. 2006); 13 – Eiffel massif, Germany (e.g. Loock et al. 1990); 14 – Monte Ragola, Appenines (Meli et al. 1996); 15 – Ivrea zone, Southern Alps (Pin 1986; Vavra et al. 1999; Quick et al. 2003; Peressini et al. 2007); 16 – Sassa, Sermenza and Mont Collon, Western Alps (Bussy et al. 1998; Monjoie et al. 2007; Baletti et al. 2012): 17 – Gruf complex, Central Alps (Galli et al. 2012); 18 – Malenco nappe, Eastern Alps (Hansmann et al. 2001; Hermann and Rubatto 2003); 19 – Sondalo gabbroic complex (Bachmann and Grauert 1981; Tribuzio et al. 1999; this study). See Fig. 11 for cumulative probability plots of ages. Sketch of the Variscan chain is modified from Martínez Catalán (2011) and Ballèvre et al. (2014)

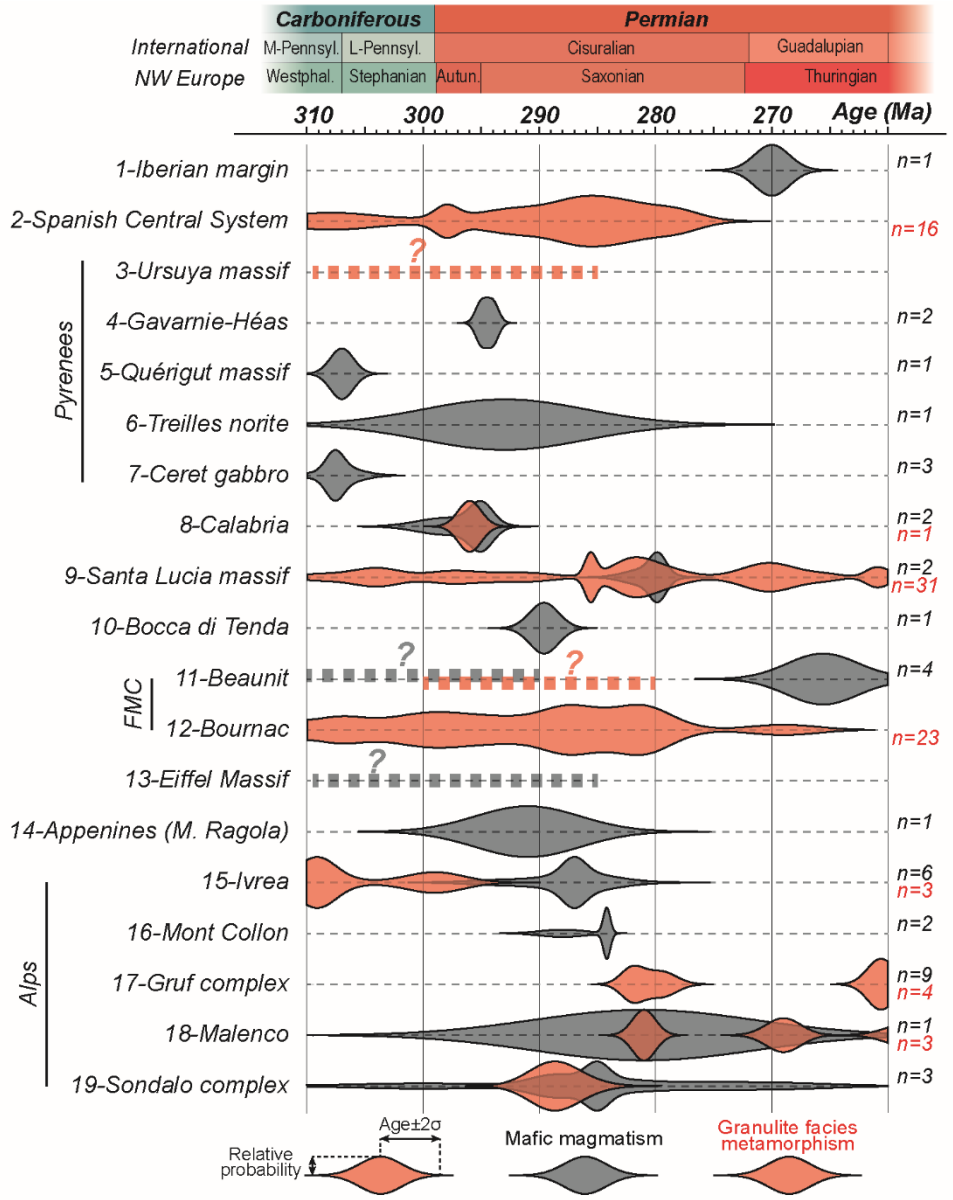

Fig. 11: Relative probability plots for U–Pb ages on zircon compiled from the literature and new ages from this study for mafic magmatism and granulitic metamorphism. Probability curves are calculated from multigrain Concordia ages and single-grain ages for Bournac granulitic metasediments, number of ages indicated by *n*. FMC stands for French Massif Central. References are indicated in the caption of Fig. 10

REFERENCES

Aguilar C, Liesa M, Castiñeiras P, Navidad M (2014) Late Variscan metamorphic and magmatic evolution in the eastern Pyrenees revealed by U–Pb age zircon dating. J Geol Soc 171:181–192.

Aguilar C, Liesa M, Štípská P, Schulmann K, Muñoz JA, Casas JM (2015) P–T–t–d evolution of orogenic middle crust of the Roc de Frausa Massif (Eastern Pyrenees): a result of horizontal crustal flow and Carboniferous doming? J Metamorph Geol 33:273–294.

Arthaud F, Matte P (1977) Late Paleozoic strike-slip faulting in the southern Europe and northern Africa: Result of a right-lateral shear zone between the Appalachians and the Urals. Geol Soc Am Bull 88:1305–1320.

Bachmann G, Grauert B (1981) Radiometrische Alterbestimmungen des Gabbro von Sondalo. Oberes Velltlin, Italienische Alpen. Fortschritte der Mineral 59:11–13.

Baletti L, Zanoni D, Spalla MI, Gosso G (2012) Structural and petrographic map of the Sassa gabbro complex (Dent Blanche nappe, Austroalpine tectonic system, Western Alps, Italy). J Maps 8:413–430.

Ballèvre M, Martínez Catalán JR, López-Carmona A, et al. (2014) Correlation of the nappe stack in the Ibero-Armorican arc across the Bay of Biscay: a joint French–Spanish project. Geol Soc London, Spec Publ. doi: 10.1144/sp405.13

Bea F, Montero P (1999) Behavior of accessory phases and redistribution of Zr, REE, Y, Th, and U during metamorphism and partial melting of metapelites in the lower crust: an example from the Kinzigite Formation of Ivrea-Verbano, NW Italy. Geochim Cosmochim Acta 63:1133–1153. doi: http://dx.doi.org/10.1016/S0016-7037(98)00292-0

Barboza SA, Bergantz GW (2000) Metamorphism and Anatexis in the Mafic Complex Contact Aureole, Ivrea Zone, Northern Italy. J Petrol 41:1307–1327. doi: 10.1093/petrology/41.8.1307

Barboza SA, Bergantz GW, Brown M (1999) Regional granulite facies metamorphism in the Ivrea zone: Is the Mafic Complex the smoking gun or a red herring? Geology 27:447–450. doi: 10.1130/0091-7613(1999)027<0447:rgfmit>2.3.co;2

Bergomi MA, Boriani A (2012) Late Neoproterozoic - Early Paleozoic accretion of the Southalpine and Austroalpine basements of Central Alps (Italy). Géologie la Fr 1:69.

Bois C, Pinet B, Roure F (1989) Dating lower crustal features in France and adjacent areas from deep seismic profiles. Prop. Process. Earth's Low. Crust. AGU, Washington, DC, pp 17–31

Bonin B, Azzouni-Sekkal A, Bussy F, Ferrag S (1998) Alkali-calcic and alkaline post-orogenic (PO) granite magmatism: petrologic constraints and geodynamic settings. Lithos 45:45–70. doi: http://dx.doi.org/10.1016/S0024-4937(98)00025-5

Boriani A, Traversi G, Del Moro A, Notarpietro A (1982) Il "granito di Brusio" (Val Poschiavo - Svizzera): caratterizzazioni chimiche, petrologiche e radiometriche. Rend Soc Ital di Mineral e Petrol 38:97–108.

Braga R, Callegari A, Messiga B, Ottolini L, Renna MR, Tribuzio R (2003) Origin of prismatine from the Sondalo granulites (Central Alps, northern Italy). Eur J Mineral 15:393–400.

Braga R, Giacomini F, Messiga B, Tribuzio R (2001) The Sondalo Gabbroic Complex (Central Alps, Northern Italy): Evidence for Emplacement of Mantle-Derived Melts into Amphibolite Facies Metapelites. Phys Chem Earth, Part A Solid Earth Geod 26:333–342.

Braga R, Massonne H-J, Morten L (2007) An early metamorphic stage for the Variscan Ulten Zone gneiss (NE Italy): evidence from mineral inclusions in kyanite. Mineral Mag 71:691–702. doi: 10.1180/minmag.2007.071.6.691

Braga R, Massonne HJ (2008) Mineralogy of inclusions in zircon from high-pressure crustal rocks from the Ulten Zone, Italian Alps. Period di Mineral 77:43–64.

Büchi H (1987) Geologie und Petrographie der Bernina IX. Das Gebiet zwischen Pontresina und dem Morteratschgletscher. Unpubl. Diplomarbeit, Univ. Zürich

Büchi H (1994) Der variskiscke Magmatismus in der östlichen Bernina. Schweizerische Mineral und Petrogr Mitteilungen 74:359–371.

Buck WR (1991) Modes of continental lithospheric extension. J Geophys Res Solid Earth 96:20161–20178. doi: 10.1029/91jb01485

Burg J-P, Van Den Drissche J, Brun J-P (1994) Syn- to post-thickening extension in the Variscan Belt of Western Europe: Modes and structural consequences. Géologie la Fr 3:33–51.

Bussy F, Venturini G, Hunziker J, Martinotti G (1998) U-Pb ages of magmatic rocks of the western Austroalpine Dent-Blanche-Sesia Unit. Schweizerische Mineral und Petrogr Mitteilungen 78:163–168.

Caby R, Jacob C (2000) La transition croûte/manteau dans la nappe de Santa-Lucia-di-Mercurio (Corse alpine): les racines d'un rift permien. Géologie la Fr 1:21–34.

Caggianelli A, Liotta D, Prosser G, Ranalli G (2007) Pressure–temperature evolution of the late Hercynian Calabria continental crust: compatibility with post-collisional extensional tectonics. Terra Nov 19:502–514. doi: 10.1111/j.1365-3121.2007.00777.x

Caggianelli A, Prosser G, Festa V, Langone A, Spiess R (2013) From the upper to the lower continental crust exposed in Calabria. 86° Congresso Nazionale della Società Geologica Italiana - Arcavacata di Rende (CS), 2012. Geol. Fielt Trips 5:

Capuzzo N, Wetzel A (2004) Facies and basin architecture of the Late Carboniferous Salvan-Dorénaz continental basin (Western Alps, Switzerland/France). Sedimentology 51:675–697. doi: 10.1111/j.1365-3091.2004.00642.x

Cassinis G, Perotti C, Ronchi A (2012) Permian continental basins in the Southern Alps (Italy) and peri-mediterranean correlations. Int J Earth Sci 101:129–157. doi: 10.1007/s00531-011-0642-6

Cassinis G, Perotti CR (2007) A stratigraphic and tectonic review of the Italian Southern Alpine Permian. Palaeoworld 16:140–172. doi: http://dx.doi.org/10.1016/j.palwor.2007.05.004

Cassinis G, Toutin-Morin N, Virgili C (1995) A General Outline of the Permian Continental Basins in Southwestern Europe. In: Scholle P, Peryt T, Ulmer-Scholle D (eds) Permian North. Pangea. Springer Berlin Heidelberg, pp 137–157

Châteauneuf JJ (1989) Esquisse paléogéographique du Permien de l'Europe de l'Ouest. Synthèse Géologique des Bassins Permiens Français Mémoire du Bur. Rech. Géologiques Minières 128:

Cocherie A, Rossi P, Fanning CM, Guerrot C (2005) Comparative use of TIMS and SHRIMP for U–Pb zircon dating of A-type granites and mafic tholeiitic layered complexes and dykes from the Corsican Batholith (France). Lithos 82:185–219. doi: http://dx.doi.org/10.1016/j.lithos.2004.12.016

Cortesogno L, Cassinis G, Dallagiovanna G, Gaggero L, Oggiano G, Ronchi A, Seno S, Vanossi M (1998) The Variscan post-collisional volcanism in Late Carboniferous–Permian sequences of Ligurian Alps, Southern Alps and Sardinia (Italy): a synthesis. Lithos 45:305–328. doi: http://dx.doi.org/10.1016/S0024-4937(98)00037-1

Costa S, Rey P (1995) Lower crustal rejuvenation and growth during post-thickening collapse: Insights from a crustal cross section through a Variscan metamorphic core complex. Geology 23:905–908. doi: 10.1130/0091-7613(1995)023<0905:lcragd>2.3.co;2

Del Moro A, Martin S, Prosser G (1999) Migmatites of the Ulten Zone (NE Italy), a Record of Melt Transfer in Deep Crust. J Petrol 40:1803–1826. doi: 10.1093/petroj/40.12.1803

Del Moro A, Notarpietro A (1987) Rb-Sr Geochemistry of some Hercynian granitoids overprinted by eo-Alpine metamorphism in the Upper Valtellina, Central Alps. Schweizerische Mineral und Petrogr Mitteilungen 67:295–306.

Del Moro A, Notarpietro A, Potenza R (1981) Revisione del significato strutturale e geocronologico delle masse intrusive minori dell'Alta Valtellina: risultati preliminari. Rend Soc Ital di Mineral e Petrol 38:89–96.

Denèle Y, Paquette J-L, Olivier P, Barbey P (2012) Permian granites in the Pyrenees: the Aya pluton (Basque Country). Terra Nov 24:105–113. doi: 10.1111/j.1365-3121.2011.01043.x

Dössegger R, Furrer H, Müller WH (1982) Die Sedimentserien der Engadiner Dolomiten und ihere lithostratigraphische Gliederung (Teil 2). Eclogae Geol Helv 75:330.

Downes H, Kempton PD, Briot D, Harmon RS, Leyreloup AF (1991) Pb and O isotope systematics in granulite facies xenoliths, French Massif Central: implications for crustal processes. Earth Planet Sci Lett 102:342–357. doi: http://dx.doi.org/10.1016/0012-821X(91)90028-G

Féménias O, Coussaert N, Bingen B, Whitehouse M, Mercier J-CC, Demaiffe D (2003) A Permian underplating event in late- to post-orogenic tectonic setting. Evidence from the mafic–ultramafic layered xenoliths from Beaunit (French Massif Central). Chem Geol 199:293–315. doi: http://dx.doi.org/10.1016/S0009-2541(03)00124-4

Fernández-Suárez J, Arenas R, Jeffries TE, Whitehouse MJ, Villaseca C (2006) A U-Pb study of zircons from a lower crustal granulite xenolith of the Spanish Central System: a record of Iberian lithospheric evolution from the Neoproterozoic to the Triassic. J Geol 114:471–783.

Feys R (1989) Introduction. Synthèse Géologique des Bassins Permiens Français Mémoire du Bur Rech Géologiques Minières 128:17–22.

Flisch M (1986) Die Hebungsgeschichte der oberostalpinen Silvretta-Decke seit der mittleren Kreide. Bull Ver Schweiz Pet-Geol Ing 53:23–49. doi: 10.5169/seals-210052

Fountain DM (1989) Growth and modification of lower continental crust in extended terrains: The Role of extension and magmatic underplating. Prop. Process. Earth's Low. Crust. AGU, Washington, DC, pp 287–299

Fountain DM, Salisbury MH (1981) Exposed cross-sections through the continental crust: implications for crustal structure, petrology, and evolution. Earth Planet Sci Lett 56:263–277. doi: http://dx.doi.org/10.1016/0012-821X(81)90133-3

Frizon de Lamotte D, Fourdan B, Leleu S, Leparmentier F, de Clarens P (2015) Style of rifting and the stages of Pangea breakup. Tectonics 34:1009–1029. doi: 10.1002/2014TC003760

Froitzheim N, Schmid SM, Conti P (1994) Repeated change from crustal shortening to orogen-parallel extension in the Austroalpine units of Graubünden. Eclogae Geol Helv 87:559–612.

Froitzheim N, Derks JF, Walter JM, Sciunnach D (2008) Evolution of an Early Permian extensional detachment fault from synintrusive, mylonitic flow to brittle faulting (Grassi Detachment Fault, Orobic Anticline, southern Alps, Italy). Geol Soc London, Spec Publ 298:69–82. doi: 10.1144/sp298.4

Furrer H (1993) Stratigraphie und Facies der Trias/Jura-Grenzschichten in den Oberostalpinen Decken Graubündens. Universität Zürich

Galli A, Le Bayon B, Schmidt MW, Burg JP, Caddick MJ, Reusser E (2011) Granulites and charnockites of the Gruf Complex: Evidence for Permian ultra-high temperature metamorphism in the Central Alps. Lithos 124:17–45. doi: http://dx.doi.org/10.1016/j.lithos.2010.08.003

Galli A, Le Bayon B, Schmidt MW, Burg JP, Reusser E, Sergeev SA, Larionov A (2012) U–Pb zircon dating of the Gruf Complex: disclosing the late Variscan granulitic lower crust of Europe stranded in the Central Alps. Contrib to Mineral Petrol 163:353–378. doi: 10.1007/s00410-011-0676-6

Galster F (2015) Accessory phases as a tool to investigate magmatic underplating in polymetamorphic metasediments: an example from a fossil lower crust: Ivrea Verbano zone, NW Italy. University of Lausanne

Gazzola D, Gosso G, Pulcrano E, Spalla MI (2000) Eo-Alpine HP metamorphism in the Permian intrusives from the steep belt of the central Alps (Languard-Campo nappe and Tonale Series). Geodin Acta 13:149–167.

Gosso G, Salvi F, Spalla MI, Zucali M (2004) Map of deformation partitioning in the polydeformed and polymetamorphic Austroalpine basement of the Central Alps (Upper Valtellina and Val Camonica, Italy). In: Pasquarè G, Venturini C, Groppelli G (eds) Mapp. Geol. Italy. APAT, Roma, pp 291–300

Guntli R, Liniger M (1989) Metamorphose in der Magma-Decke im Bereich Piz da la Margna und Piz Fedoz (Oberengadin). Schweizerische Mineral und Petrogr Mitteilungen 69:289–301.

Halmes C (1991) Petrographische und geochemische Untersuchungen am Err-Kristallin zwischen St. Moritz und dem Val Bever (Engadin, Graubünden). University of Bern, Lizentiarbeit

Handy MR (1996) The transition from passive to active margin tectonics: a case study from the zone of Samedan (eastern Switzerland). Geol Rundschau 85:832–851. doi: 10.1007/BF02440114

Hansmann W, Müntener O, Hermann J (2001) U-Pb zircon geochronology of a tholeiitic intrusion and associated migmatites at a continental crust-mantle transition, Val Malenco, Italy. Schweizerische Mineral und Petrogr Mitteilungen 81:239–255.

Hanson GN, El Tahlawi MR, Weber W (1966) K-Ar and Rb-Sr ages of pegmatites in the South Central Alps. Earth Planet Sci Lett 1:407–413.

Harley SL (1989) The origins of granulites: a metamorphic perspective. Geol Mag 126:215–247.

Henk A (1999) Did the Variscides collapse or were they torn apart?: A quantitative evaluation of the driving forces for post-convergent extension in central Europe. Tectonics 18:774–792.

Hermann J, Müntener O, Günther D (2001) Differentiation of Mafic Magma in a Continental Crust-to-Mantle Transition Zone. J Petrol 42:189–206. doi: 10.1093/petrology/42.1.189

Hermann J, Müntener O, Trommsdorff V, Hansmann W, Piccardo GB (1997) Fossil crust-to-mantle transition, Val Malenco (Italian Alps). J Geophys Res Solid Earth 102:20123–20132. doi: 10.1029/97jb01510

Hermann J, Rubatto D (2003) Relating zircon and monazite domains to garnet growth zones: age and duration of granulite facies metamorphism in the Val Malenco lower crust. J Metamorph Geol 21:833–852. doi: 10.1046/j.1525-1314.2003.00484.x

Hoinkes G, Thöni M (1993) Evolution of the Ötztal-Stubai, Scarl-Campo and Ulten Basement Units. In: Raumer JF, Neubauer F (eds) Pre-Mesozoic Geol. Alps. Springer Berlin Heidelberg, Berlin Heidelberg, pp 485–494

Hoskin PWO, Schaltegger U (2003) The composition of zircon and igneous and metamorphic petrogenesis. Rev Mineral Geochemistry 53:27–62.

Kilzi MA, Grégoire M, Bosse V, Benoît M, Driouch Y, de Saint Blanquat M, Debat P (2016) Geochemistry and zircon U–Pb geochronology of the ultramafic and mafic rocks emplaced within the anatectic series of the Variscan Pyrenees: The example of the Gavarnie–Heas dome (France). Comptes Rendus Geosci 348:107–115. doi: http://dx.doi.org/10.1016/j.crte.2015.06.014

Koenig MA (1964) Geologisch-petrographische Untersuchungen im oberen Veltlin. PhD thesis, Universität Zurich

Langone A, Braga R, Massonne H-J, Tiepolo M (2011) Preservation of old (prograde metamorphic) U–Th–Pb ages in unshielded monazite from the high-pressure paragneisses of the Variscan Ulten Zone (Italy). Lithos 127:68–85. doi: http://dx.doi.org/10.1016/j.lithos.2011.08.007

Lardeaux JM, Spalla MI (1991) From granulites to eclogites in the Sesia zone (Italian Western Alps): a record of the opening and closure of the Piedmont ocean. J Metamorph Geol 9:35–59. doi: 10.1111/j.1525-1314.1991.tb00503.x

Libourel G (1988) Le complexe de Santa-Lucia di Mercurio (Corse): un équivalent possible des complexes de la Zone d'Ivrée. Comptes Rendus l'Académie des Sci - Ser IIA - Earth Planet Sci 307:1225–1230.

Libourel G (1985) Le complexe de Santa Lucia di Mercurio (Corse): Ultramafites mantelliques, intrusion basique stratifiée, paragneiss granulitique. Un équivalent possibe des complexes de la zone d'Ivrée. PhD Thesis, Université Paul Sabatier de Toulouse

Linnen RL, Keppler H (2002) Melt composition control of Zr/Hf fractionation in magmatic processes. Geochim Cosmochim Acta 66:3293–3301. doi: http://dx.doi.org/10.1016/S0016-7037(02)00924-9

Loock G, Stosch HG, Seck HA (1990) Granulite facies lower crustal xenoliths from the Eifel, West Germany: petrological and geochemical aspects. Contrib to Mineral Petrol 105:25–41. doi: 10.1007/bf00320964

Lorenz V, Nicholls IA (1976) The Permocarboniferous Basin and Range Province of Europe. An Application op Plate Tectonics. In: Falke H (ed) Cont. Permain Cent. West, South Eur. Springer Netherlands, pp 313–342

Lorenz V, Nicholls IA (1984) Plate and intraplate processes of Hercynian Europe during the late paleozoic. Tectonophysics 107:25–56. doi: http://dx.doi.org/10.1016/0040-1951(84)90027-1

Ludwig KR (2012) Isoplot v. 3.75: A Geochronological Toolkit for Microsoft Excel.

Maggetti M, Flisch M (1993) Evolution of the Silvretta Nappe. In: von Raumer JF, Neubauer F (eds) Pre-Mesozoic Geol. Alps. Springer Berlin Heidelberg, pp 469–484

Manatschal G, Froitzheim N, Rubenach M, Turrin BD (2001) The role of detachment faulting in the formation of an ocean-continent transition: insights from the Iberia Abyssal Plain. Geol Soc London, Spec Publ 187:405–428. doi: 10.1144/gsl.sp.2001.187.01.20

Manzotti P, Zucali M (2013) The pre-Alpine tectonic history of the Austroalpine continental basement in the Valpelline unit (Western Italian Alps). Geol Mag 150:153–172. doi: doi:10.1017/S0016756812000441

Martínez Catalán JR (2011) Are the oroclines of the Variscan belt related to late Variscan strike-slip tectonics? Terra Nov 23:241–247.

Marquer D, Challandes N, Schaltegger U (1998) Early Permian magmatism in Briançonnais terranes: Truzzo granite and Roffna rhyolite (eastern Penninic nappes, Swiss and Italian Alps). Schweizerische Mineral und Petrogr Mitteilungen 78:397–414.

McCarthy A, Müntener O (2015) Ancient depletion and mantle heterogeneity: Revisiting the Permian-Jurassic paradox of Alpine peridotites. Geol . doi: 10.1130/G36340.1

Meier A (2003) The Periadriatic Fault System in Valtellina (N-Italy) and the Evolution of the Southwestern Segment of the Eastern Alps. PhD Thesis, ETH Zurich

Meli S, Montanini A, Thöni M, Frank W (1996) Age of mafic granulite blocks from the External Liguride Units (Northern Apennines, Italy). Mem di Sci Geol 48:65–72.

Mohn G, Manatschal G, Beltrando M, Masini E, Kusznir N (2012) Necking of continental crust in magma-poor rifted margins: Evidence from the fossil Alpine Tethys margins. Tectonics 31:1–28.

Mohn G, Manatschal G, Masini E, Müntener O (2011) Rift-related inheritance in orogens: a case study from the Austroalpine nappes in Central Alps (SE-Switzerland and N-Italy). Int J Earth Sci 100:937–961. doi: 10.1007/s00531-010-0630-2

Mohn G, Manatschal G, Müntener O, Beltrando M, Masini E (2010) Unravelling the interaction between tectonic and sedimentary processes during lithospheric thinning in the Alpine Tethys margins. Int J Earth Sci 99:75–101. doi: 10.1007/s00531-010-0566-6

Monjoie P, Bussy F, Schaltegger U, Mulch A, Lapierre H, Pfeifer H-R (2007) Contrasting magma types and timing of intrusion in the Permian layered mafic complex of Mont

Collon (Western Alps, Valais, Switzerland): evidence from U/Pb zircon and 40Ar/39Ar amphibole dating. Swiss J Geosci 100:125–135. doi: 10.1007/s00015-007-1210-8

Müntener O, Hermann J (2001) The role of lower crust and continental upper mantle during formation of non-volcanic passive margins: evidence from the Alps. Geol Soc London, Spec Publ 187:267–288. doi: 10.1144/gsl.sp.2001.187.01.13

Müntener O, Hermann J, Trommsdorff V (2000) Cooling History and Exhumation of Lower-Crustal Granulite and Upper Mantle (Malenco, Eastern Central Alps). J Petrol 41:175–200. doi: 10.1093/petrology/41.2.175

Müntener O, Pettke T, Desmurs L, Meier M, Schaltegger U (2004) Refertilization of mantle peridotite in embryonic ocean basins: trace element and Nd isotopic evidence and implications for crust–mantle relationships. Earth Planet Sci Lett 221:293–308. doi: http://dx.doi.org/10.1016/S0012-821X(04)00073-1

Murali A V, Parthasarathy R, Mahadevan TM, Das MS (1983) Trace element characteristics, REE patterns and partition coefficients of zircons from different geological environments—A case study on Indian zircons. Geochim Cosmochim Acta 47:2047–2052. doi: http://dx.doi.org/10.1016/0016-7037(83)90220-X

Paquette J-L, Ménot R-P, Pin C, Orsini J-B (2003) Episodic and short-lived granitic pulses in a post-collisional setting: evidence from precise U–Pb zircon dating through a crustal cross-section in Corsica. Chem Geol 198:1–20. doi: http://dx.doi.org/10.1016/S0009-2541(02)00401-1

Peressini G, Quick JE, Sinigoi S, Hofmann AW, Fanning M (2007) Duration of a Large Mafic Intrusion and Heat Transfer in the Lower Crust: a SHRIMP U–Pb Zircon Study in the Ivrea–Verbano Zone (Western Alps, Italy). J Petrol 48:1185–1218. doi: 10.1093/petrology/egm014

Petri B (2014) Formation and exhumation of Permian granulites: establishing the pre-rift conditions and determining the syn-rift exhumation history. PhD thesis, University of Strasbourg

Petri B, Mohn G, Štípská P, Schulmann K, Manatschal G (2016) The Sondalo gabbro contact aureole (Campo unit, Eastern Alps): implications for mid-crustal mafic magma emplacement. Contrib to Mineral Petrol 171:52. doi: 10.1007/s00410-016-1263-7

Pin C (1986) Datation U-Pb sur zircons à 285 M.a. du complexe gabbro-dioritique du Val Sesia-Val Mastallone et âge tardi-hercynien du métamorphisme granulitique de la zone Ivrea-Verbano (Italie). Comptes Rendus l'Académie des Sci Série 2 Sci la Terre des planètes 9:827–830.

Quick JE, Sinigoi S, Snoke AW, Kalakay TJ, Mayer A, Peressini G (2003) Geologic map of the southern Ivrea-Verbano Zone, northwestern Italy: U.S. Geological Survey Geologic Investigations Series Map I-2776, scale 1:25,000. 22 p.

Rageth R (1984) Intrusiva und Extrusiva der Bernina-Decke zwischen Morteratsch und Berninapass (Graubünden). Schweizerische Mineral und Petrogr Mitteilungen 64:83–109.

Rampone E, Hofmann AW, Raczek I (1998) Isotopic contrasts within the Internal Liguride ophiolite (N. Italy): the lack of a genetic mantle–crust link. Earth Planet Sci Lett 163:175–189. doi: http://dx.doi.org/10.1016/S0012-821X(98)00185-X

Redler C, White RW, Johnson TE (2013) Migmatites in the Ivrea Zone (NW Italy): Constraints on partial melting and melt loss in metasedimentary rocks from Val Strona di Omegna. Lithos 175–176:40–53. doi: http://dx.doi.org/10.1016/j.lithos.2013.04.019

Rey P, Vanderhaeghe O, Teyssier C (2001) Gravitational collapse of the continental crust: definition, regimes and modes. Tectonophysics 342:435–449. doi: http://dx.doi.org/10.1016/S0040-1951(01)00174-3

Roberts MP, Pin C, Clemens JD, Paquette J-L (2000) Petrogenesis of Mafic to Felsic Plutonic Rock Associations: the Calc-alkaline Quérigut Complex, French Pyrenees. J Petrol 41:809–844.

Rossi P, Cocherie A, Fanning CM, Deloule É (2006) Variscan to eo-Alpine events recorded in European lower-crust zircons sampled from the French Massif Central and Corsica, France. Lithos 87:235–260. doi: http://dx.doi.org/10.1016/j.lithos.2005.06.009

Royden L, Keen CE (1980) Rifting process and thermal evolution of the continental margin of Eastern Canada determined from subsidence curves. Earth Planet Sci Lett 51:343–361. doi: http://dx.doi.org/10.1016/0012-821X(80)90216-2

Rubatto D (2002) Zircon trace element geochemistry: partitioning with garnet and the link between U–Pb ages and metamorphism. Chem Geol 184:123–138. doi: http://dx.doi.org/10.1016/S0009-2541(01)00355-2

Rudnick RL, Fountain DM (1995) Nature and composition of the continental crust: a lower crustal perspective. Rev Geophys 33:267–309.

Schaltegger U, Brack P (2007) Crustal-scale magmatic systems during intracontinental strike-slip tectonics: U, Pb and Hf isotopic constraints from Permian magmatic rocks of the Southern Alps. Int J Earth Sci 96:1131–1151. doi: 10.1007/s00531-006-0165-8

Schaltegger U, Fanning CM, Günther D, Maurin JC, Schulmann K, Gebauer D (1999) Growth, annealing and recrystallization of zircon and preservation of monazite in high-grade metamorphism: conventional and in-situ U-Pb isotope, cathodoluminescence and microchemical evidence. Contrib to Mineral Petrol 134:186–201. doi: 10.1007/s004100050478

Schaltegger U, Gebauer D (1999) Pre-Alpine geochronology of the Central, Western and Southern Alps. Schweizerische Mineral und Petrogr Mitteilungen 79:79–87.

Schenk V (1980) U-Pb and Rb-Sr radiometric dates and their correlation with metamorphic events in the granulite-facies basement of the serre, Southern Calabria (Italy). Contrib to Mineral Petrol 73:23–38. doi: 10.1007/BF00376258

Schmid S, Fügenschuh B, Kissling E, Schuster R (2004) Tectonic map and overall architecture of the Alpine orogen. Eclogae Geol Helv 97:93–117. doi: 10.1007/s00015-004-1113-x

Schmid SM, Haas R (1989) Transition from near-surface thrusting to Intrabasement Decollement, Schlinig Thrust, eastern Alps. Tectonics 8:697–718. doi: 10.1029/TC008i004p00697

Schuster R, Scharbert S, Abart R, Frank W (2001) Permo-Triassic extension and related HT/LP metamorphism in the Austroalpine-Southalpine realm. Mitteilungen der Geol und Bergbau Studenten Österreichs 44:111–141.

Schuster R, Stüwe K (2008) Permian metamorphic event in the Alps. Geology 36:603–606.

Sinigoi S, Quick JE, Demarchi G, Klötzli US (2016) Production of hybrid granitic magma at the advancing front of basaltic underplating: Inferences from the Sesia Magmatic System (south-western Alps, Italy). Lithos 252–253:109–122. doi: http://dx.doi.org/10.1016/j.lithos.2016.02.018

Sölva H, Thöni M, Habler G (2003) Dating a single garnet crystal with very high Sm/Nd ratios (Campo basement unit, Eastern Alps). Eur J Mineral 15:35–42.

Spalla MI, Zanoni D, Marotta AM, Rebay G, Roda M, Zucali M, Gosso G (2014) The transition from Variscan collision to continental break-up in the Alps: insights from the comparison between natural data and numerical model predictions. Geol Soc London, Spec Publ. doi: 10.1144/sp405.11

Spillmann P, Büchi HJ (1993) The Pre-Alpine Basement of the Lower Austro-Alpine Nappes in the Bernina Massif (Grisons, Switzerland; Valtellina, Italy). In: von Raumer JF, Neubauer F (eds) Pre-Mesozoic Geol. Alps. Springer Berlin Heidelberg, pp 457–467

Stacey JS, Kramers JD (1975) Approximation of terrestrial lead isotope evolution by a two-stage model. Earth Planet Sci Lett 26:207–221. doi: http://dx.doi.org/10.1016/0012-821X(75)90088-6

Stampfli GM (1996) The Intra-Alpine terrain: A Paleotethyan remnant in the Alpine Variscides. Eclogae Geol Helv 89:13–42.

Staub R (1946) Geologische Karte der Berninagruppe und ihrer Umgebung im Oberengadin, Bergell, Val Malenco, Puschlav und Livigno, scale 1:50,000. Speziale Karte 118, Schweizerische Geol. Kommission

Stepanov AS, Hermann J (2013) Fractionation of Nb and Ta by biotite and phengite: Implications for the "missing Nb paradox." Geology. doi: 10.1130/g33781.1

Stipp M, Stünitz H, Heilbronner R, Schmid SM (2002) The eastern Tonale fault zone: a "natural laboratory" for crystal plastic deformation of quartz over a temperature range from 250 to 700 °C. J Struct Geol 24:1861–1884.

Sun S -s., McDonough WF (1989) Chemical and isotopic systematics of oceanic basalts: implications for mantle composition and processes. Geol Soc London, Spec Publ 42:313–345. doi: 10.1144/gsl.sp.1989.042.01.19

Thöni M (1981) Degree and evolution of the alpine metamorphism in the Austroalpine unit W of the Hohe Tauern in the light of K/Ar and Rb/Sr age determination on micas. Jahrb der Geol Bundesanstalt 124:111–174.

Thybo H, Artemieva IM (2013) Moho and magmatic underplating in continental lithosphere. Tectonophysics 609:605–619. doi: http://dx.doi.org/10.1016/j.tecto.2013.05.032

Timmerman MJ (2004) Timing, geodynamic setting and character of Permo-Carboniferous magmatism in the foreland of the Variscan Orogen, NW Europe. Geol Soc London, Spec Publ 223:41–74. doi: 10.1144/gsl.sp.2004.223.01.03

Tribuzio R, Renna MR, Braga R, Dallai L (2009) Petrogenesis of Early Permian olivine-bearing cumulates and associated basalt dykes from Bocca di Tenda (Northern Corsica): Implications for post-collisional Variscan evolution. Chem Geol 259:190–203. doi: http://dx.doi.org/10.1016/j.chemgeo.2008.10.045

Tribuzio R, Thirlwall MF, Messiga B (1999) Petrology, mineral and isotope geochemistry of the Sondalo gabbroic complex (Central Alps, Northern Italy): implications for the origin

of post-Variscan magmatism. Contrib to Mineral Petrol 136:48–62. doi: 10.1007/s004100050523

Trommsdorff V, Montrasio A, Hermann J, Müntener O, Spillmann P, Gieré R (2005) The Geological Map of Valmalenco. Schweizerische Mineral und Petrogr Mitteilungen 85:1–13.

Trümpy R, Dössegger R (1972) Permian of Switzerland. In: Brill E (ed) Rotliegend; essays Eur. Low. Permian. Leiden, pp 189–215

Vanderhaeghe O, Teyssier C (2001) Partial melting and flow of orogens. Tectonophysics 342:451–472. doi: http://dx.doi.org/10.1016/S0040-1951(01)00175-5

Vavra G, Schmid R, Gebauer D (1999) Internal morphology, habit and U-Th-Pb microanalysis of amphibolite-to-granulite facies zircons: geochronology of the Ivrea Zone (Southern Alps). Contrib to Mineral Petrol 134:380–404. doi: 10.1007/s004100050492

Vielzeuf D (1984) Relations de phases dans le faciès granulite et implications géodynamiques. L'exemple des granulites des Pyrénées. PhD Thesis, Université de Clermont II

Vielzeuf D, Kornprobst J (1984) Crustal splitting and the emplacement of Pyrenean lherzolites and granulites. Earth Planet Sci Lett 67:87–96.

Vielzeuf D, Pin C (1991) Granulites orthodérivées d'âge tardi-hercynien; exemple de la norite de Treilles, Corbières (Aude, France). Bull la société géologique Fr 162:1057–1066.

Villa IM, Hermann J, Müntener O, Trommsdorff V (2000) 39Ar−40Ar dating of multiply zoned amphibole generations (Malenco, Italian Alps). Contrib to Mineral Petrol 140:363–381. doi: 10.1007/s004100000197

Villaseca C, Orejana D, Paterson BA, Billstrom K, Pérez-Soba C (2007) Metaluminous pyroxene-bearing granulite xenoliths from the lower continental crust in central Spain: their role in the genesis of Hercynian I-type granites. Eur J Mineral 19:463–477. doi: 10.1127/0935-1221/2007/0019-1746

Viola G, Mancktelow NS, Seward D, Meier A, Martin S (2003) The Pejo fault system: An example of multiple tectonic activity in the Italian Eastern Alps. Geol Soc Am Bull 115:515–532.

Von Quadt A, Grünenfelder M, Büchi H (1994) U-Pb zircon ages from igneous rocks of the Bernina nappe system (Grisons, Switzerland). Schweizerische Mineral und Petrogr Mitteilungen 74:373–382.

Voshage H, Hunziker JC, Hofmann AW, Zingg A (1987) A Nd and Sr isotopic study of the Ivrea zone, Southern Alps, N-Italy. Contrib to Mineral Petrol 97:31–42. doi: 10.1007/bf00375212

Whitney DL, Teyssier C, Rey P, Buck WR (2012) Continental and oceanic core complexes. Geol Soc Am Bull. doi: 10.1130/b30754.1

Wilson M, Neumann E-R, Davies GR, Timmerman MJ, Heeremans M, Larsen BT (2004) Permo-Carboniferous magmatism and rifting in Europe: introduction. Geol Soc London, Spec Publ 223:1–10. doi: 10.1144/gsl.sp.2004.223.01.01

Xiong X, Keppler H, Audétat A, Ni H, Sun W, Li Y (2011) Partitioning of Nb and Ta between rutile and felsic melt and the fractionation of Nb/Ta during partial melting of hydrous metabasalt. Geochim Cosmochim Acta 75:1673–1692. doi: http://dx.doi.org/10.1016/j.gca.2010.06.039